© 2015. Published by The Company of Biologists Ltd | Development (2015) 142, 1418-1430 doi:10.1242/dev.109496

RESEARCH ARTICLE

STEM CELLS AND REGENERATION

Brg1 modulates enhancer activation in mesoderm lineage commitment

Jeffrey M. Alexander[1,2], Swetansu K. Hota[1,2], Daniel He[1,2], Sean Thomas[1,2], Lena Ho[3], Len A. Pennacchio[4,5] and Benoit G. Bruneau[1,2,6,7,*]

ABSTRACT

The interplay between different levels of gene regulation in modulating developmental transcriptional programs, such as histone modifications and chromatin remodeling, is not well understood. Here, we show that the chromatin remodeling factor *Brg1* is required for enhancer activation in mesoderm induction. In an embryonic stem cell-based directed differentiation assay, the absence of Brg1 results in a failure of cardiomyocyte differentiation and broad deregulation of lineage-specific gene expression during mesoderm induction. We find that Brg1 co-localizes with H3K27ac at distal enhancers and is required for robust H3K27 acetylation at distal enhancers that are activated during mesoderm induction. *Brg1* is also required to maintain Polycomb-mediated repression of non-mesodermal developmental regulators, suggesting cooperativity between Brg1 and Polycomb complexes. Thus, *Brg1* is essential for modulating active and repressive chromatin states during mesoderm lineage commitment, in particular the activation of developmentally important enhancers. These findings demonstrate interplay between chromatin remodeling complexes and histone modifications that, together, ensure robust and broad gene regulation during crucial lineage commitment decisions.

KEY WORDS: Chromatin, Enhancers, Gene expression, Histone modification, Mesoderm, Stem cells

INTRODUCTION

The emergence of individual cell types during development relies on the correct sets of genes becoming activated, while inappropriate sets of genes are simultaneously repressed. This process is achieved in large part by modifying chromatin structure, which packages the genome within the nucleus and affects multiple facets of gene regulation (Ho and Crabtree, 2010).

Histone modifications annotate the genome by marking active, repressed and other functional domains singly or in combination (Zhou et al., 2011). For example, trimethylation of histone H3 lysine 27 (H3K27me3), deposited by the Polycomb repressive complex 2 (PRC2), is associated with gene silencing (Surface et al., 2010). In embryonic stem cells (ESCs), PRC2 targets a broad group of developmental regulators for silencing to ensure appropriate lineage-specific gene expression (Surface et al., 2010). Conversely, acetylated histone H3 lysine 27 (H3K27ac) is a hallmark of active chromatin and, in particular, of enhancers, non-coding DNA elements that regulate tissue-specific gene expression patterns (Calo and Wysocka, 2013). Enhancer occupancy by H3K27ac is highly dynamic during cellular differentiation, yet the factors that modulate H3K27ac occupancy at promoters and enhancers remain poorly understood.

Eukaryotes use ATP-dependent chromatin remodelers to unwind, slide and/or evict individual nucleosomes (Ho and Crabtree, 2010; Wu et al., 2009). In mammals, the Swi/Snf-like Brg1/Brm-associated factor (BAF) chromatin-remodeling complexes include 10-12 interchangeable subunits and function in regulating cell-cycle progression, DNA repair and development (Ho and Crabtree, 2010). Remodeling activity is mediated by the ATPase subunit, which is encoded by either *Brg1* (also known as *Smarca4*) or the related gene *Brm* (also known as *Smarca2*). *Brg1* is essential for embryonic development and maintenance of pluripotency, whereas *Brm* knockout mice are viable (Bultman et al., 2000; Ho et al., 2009; Reyes et al., 1998), arguing that *Brg1* is the consequential ATPase during development. *Brg1* is required in numerous tissue and cell types *in vivo* (Ho and Crabtree, 2010), including multiple cell types within the cardiac lineage (Hang et al., 2010; Stankunas et al., 2008; Takeuchi and Bruneau, 2009; Takeuchi et al., 2011). How BAF complexes function to regulate gene expression within these cell lineages is still poorly understood.

A comprehensive picture of *Brg1* function during development necessitates detailed understanding not only of the regulatory loci bound by Brg1 but also its functional activity at these regions, including how this activity facilitates the transitions between distinct chromatin states – marked by histone modifications – that occur during cell differentiation. Such questions bear on fundamental features of chromatin regulation, namely how epigenetic modification and chromatin remodeling are deployed during development to modify the chromatin template in a coordinated fashion. Brg1 is found at distal regulatory regions (Euskirchen et al., 2011; Hu et al., 2011; Morris et al., 2014; Rada-Iglesias et al., 2011; Yu et al., 2013), but the role of Brg1 at these regions remains poorly understood. Here, we investigate the function of *Brg1* during embryonic stem cell differentiation. We find that loss of *Brg1* leads to disruption of cardiomyocyte differentiation and dysregulation of lineage-specific gene expression during mesoderm induction. Furthermore, we find that *Brg1* is required for robust H3K27 acetylation, predominately at distal enhancers that transition from inactive to active states during mesoderm induction. *Brg1* is also required to maintain Polycomb-mediated repression of non-mesodermal developmental regulators through deposition of H3K27me3, suggesting cooperativity between Brg1 and Polycomb complexes.

[1]Gladstone Institute of Cardiovascular Disease, San Francisco, CA 94158, USA. [2]Roddenberry Center for Stem Cell Biology and Medicine at Gladstone, San Francisco, CA 94158, USA. [3]Institute of Medical Biology, A*STAR, Singapore 138648. [4]Genomics Division, Lawrence Berkeley National Laboratory, Berkeley, CA 94720, USA. [5]United States Department of Energy, Joint Genome Institute, Walnut Creek, CA 94598, USA. [6]Department of Pediatrics, University of California, San Francisco, CA 94143, USA. [7]Cardiovascular Research Institute, University of California, San Francisco, CA 94158, USA.

*Author for correspondence (bbruneau@gladstone.ucsf.edu)

Received 25 February 2014; Accepted 27 February 2015

Development (2015) 142, 1418-1430 doi:10.1242/dev.109496

RESULTS

Essential BAF complex subunits are enriched at early stages of cardiac differentiation

To gain deeper insight into how chromatin is regulated during cardiac differentiation, we analyzed our published expression datasets (Wamstad et al., 2012) to identify the expression patterns of known chromatin regulators. We selected genes annotated with involvement in chromatin remodeling (Gene ontology category GO0006338) or covalent chromatin modification (GO00016569), and clustered their gene expression patterns across four stages of cardiomyocyte differentiation: ESCs, mesodermal precursors (MES), cardiac precursors (CP) or functional cardiomyocytes (CMs) (supplementary material Table S1). This analysis classified chromatin regulators into three expression patterns (Fig. 1A). We identified one cluster with high expression in ESCs and reduced expression upon exit of the pluripotent state. Within this group were the *de novo* DNA methyltransferase *Dnmt3b*, which modulates DNA methylation levels in the early mouse embryo (Okano et al., 1999), and *Dpy30*, a member of MLL family complexes that is required for differentiation of ESCs (Jiang et al., 2011) (Table 1). Expression in a second cluster peaked at the MES stage, followed by downregulation in differentiated CMs. Many BAF complex subunits demonstrated this expression pattern, including the essential core subunits *Baf57* (*Smarce1* – Mouse Genome Informatics) and *Baf47* (*Smarcb1* – Mouse Genome Informatics) and the enzymatic subunit *Brg1* (Ho and Crabtree, 2010; Wu et al., 2009). The last expression cluster demonstrated increased CM expression; within this group were *Smyd1*, a known regulator of cardiac development (Gottlieb et al., 2002); *Hdac9*, which modulates the hypertrophic response (Zhang et al., 2002); and *Jmjd3* (*Kdm6b* – Mouse Genome Informatics), a histone H3 lysine 27 demethylase. This cluster also contained multiple components of BAF complexes, including *Baf60c* (*Smarcd3* – Mouse Genome Informatics), *Brm*, *Baf170* (*Smarcc2* – Mouse Genome Informatics), *Baf45c* (*Dpf3* – Mouse Genome Informatics), *Baf45d* and *Baf250b* (*Arid1b* – Mouse Genome Informatics), suggesting that BAF complexes undergo subunit switching during cardiomyocyte differentiation analogous to that observed in the nervous system (Ho and Crabtree, 2010; Wu et al., 2009).

Brg1 is required to induce mesoderm and cardiac markers from embryonic stem cells

Dynamic expression of BAF complex subunits suggested that these complexes play distinct roles at different stages of cardiac differentiation. We confirmed that Brg1 protein is more abundant

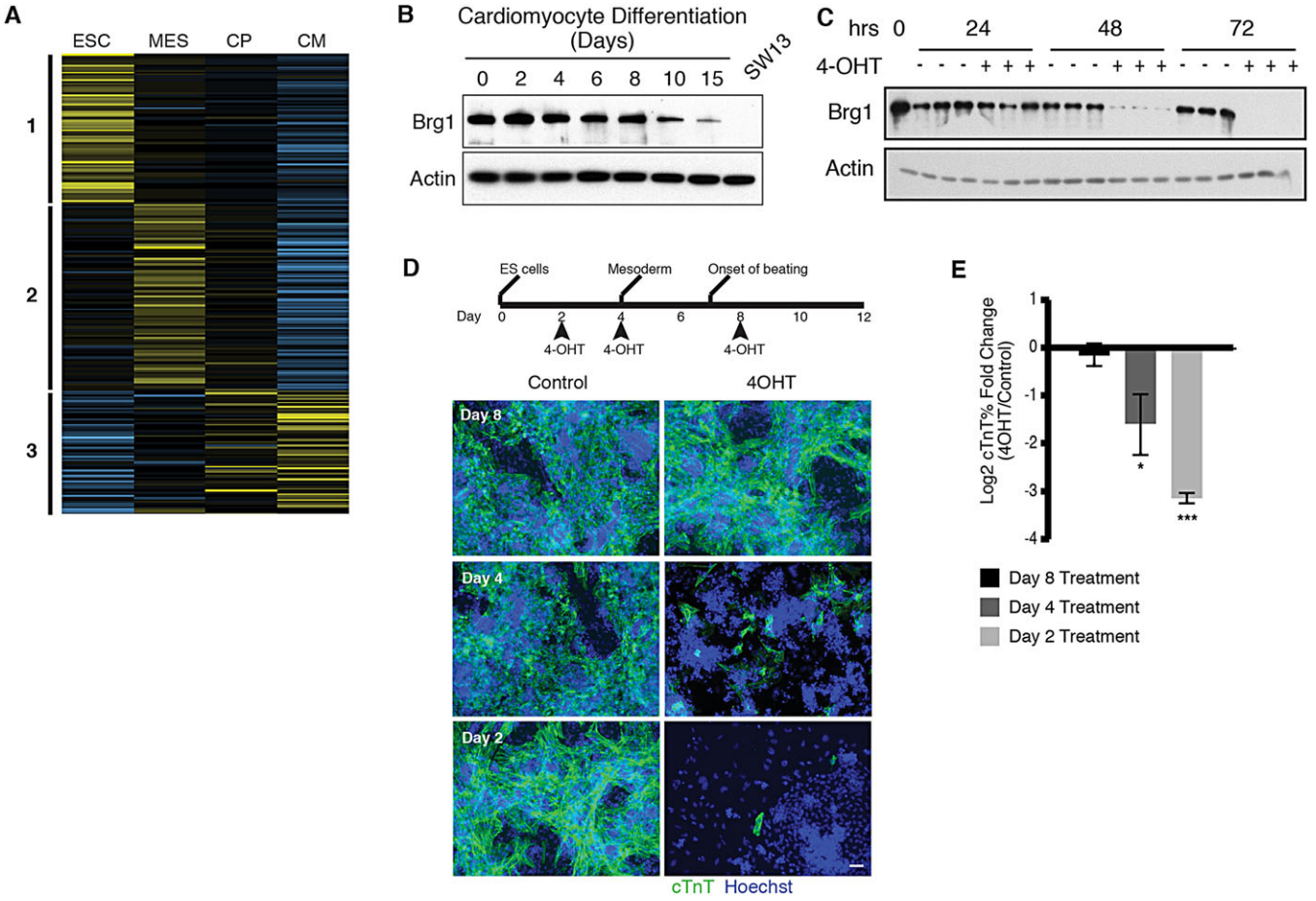

Fig. 1. *Brg1* is required for directed differentiation of ESCs to cardiomyocytes (CMs). (A) Heat map representation of clustering analysis of RNA expression of chromatin regulators at four stages of directed CM differentiation identifies three expression patterns. Chromatin regulators include genes annotated with GO terms GO0006338 and GO00016569 and additional known regulators. (B) Western blot analysis demonstrates reduced abundance of Brg1 at late stages of CM differentiation. Lysate from the adrenal carcinoma SW13, which does not express Brg1, was used as a negative control. Actin was used as a loading control. (C) Western blot analysis of a 4-OHT treatment time course in *Brg1$^{f/f}$; Actin-CreER* ESCs. Loss of Brg1 expression is near complete after 48 h of 4-OHT treatment. (D) Control (vehicle only, THF) or 4-OHT was added after 2, 4 and 8 days of differentiation to mediate *Brg1* deletion, and the presence of cardiomyocytes was determined by immunofluorescence for cTnT at day 12. Scale bar: 50 µm. (E) Comparison of percentage of cTnT^{+} cells for control or 4-OHT-treated cultures measured by flow cytometry. *P<0.05, ***P<0.001; one-sample t-test.

Development (2015) 142, 1418-1430 doi:10.1242/dev.109496

Table 1. Example genes for chromatin regulators found in expression clusters identified in Figure 1A

Cluster 1	*Dnmt3b*, *Ino80*, *Suz12* MLL complex: *Rbbp5*, *Dpy30*, *Wdr5*
Cluster 2	BAF complex: *Baf45a*, *Baf60a/b*, *Baf47*, *Baf57*, *Baf200*, *Baf180*, *Brg1**, *Baf53a*, *Baf155*
Cluster 3	*Hdac9*, *Smyd1*, *Jmjd3* BAF complex: *Baf60c*, *Brm**, *Baf170*, *Baf45c/d*, *Baf250b*

*ATPase subunit.

at early stages of cardiac differentiation than in late-stage cultures enriched for differentiated CMs (Fig. 1B). The enrichment of *Brg1* in mesoderm precursors suggested that BAF complexes perform a broad and uncharacterized function in the early progenitors of the cardiac lineage.

To investigate the function of *Brg1* at distinct stages of cardiac differentiation, we used directed CM differentiation (see supplementary material Methods) in a mouse ESC line with two floxed alleles of *Brg1* and a constitutively expressed Cre recombinase-estrogen receptor fusion protein (*Brg1*$^{f/f}$;*Actin-CreER*) (Ho et al., 2011, 2009). Adding 4-hydroxytamoxifen (4-OHT) led to efficient deletion of the floxed allele and loss of Brg1 protein, which was near-complete 48 h after 4-OHT treatment and undetectable by 72 h (Fig. 1C). Treatment of differentiating cultures with 4-OHT allowed for controlled deletion of *Brg1* at specific stages of differentiation and allowed for the comparison of control and treatment groups within a single differentiation, which limited confounding effects from differentiation variability. We added 4-OHT at three time points: during the induction of MES (day 2), as mesodermal precursors are differentiating towards CMs (day 4), and after the appearance of beating CMs (day 8) (Fig. 1D). Cultures treated with 4-OHT at day 8 showed no discernable differences from control cultures: they continued to contract many days after addition of 4-OHT and had comparable numbers of cardiac troponin T (cTnT; Tnnt2 – Mouse Genome Informatics)-positive CMs (Fig. 1D,E). By contrast, cultures treated with 4-OHT at day 2 or day 4 had fewer cTnT^{+} CMs than controls. This was most striking in cultures treated with 4-OHT at day 2, which had a near-complete loss of cTnT^{+} CMs. Whereas control-treated cultures expand to generate dense layers, containing multiple fibers of interconnected CMs after mesoderm induction, cultures treated with 4-OHT at day 2 failed to expand in these conditions, giving rise to a sparse monolayer of differentiated cells (supplementary material Fig. S1A,B). Treatment of wild-type ESCs undergoing the same differentiation protocol with 4-OHT did not affect their ability to differentiate (supplementary material Fig. S1C). Thus, *Brg1* is required for the differentiation of embryonic stem cells to CMs.

As addition of 4-OHT at day 2 would lead to deletion of *Brg1* during mesoderm induction, we examined mesodermal markers during differentiation of ESCs. We differentiated *Brg1*$^{f/f}$;*Actin-CreER* ESCs for 2 days as embryoid bodies (EBs) in serum-free medium and induced MES by treating these cultures with Vegf, activin A (Inhba – Mouse Genome Informatics) and Bmp4 in the presence of 4-OHT or vehicle control for 40 h, analogous to the first 4 days of our directed CM differentiation protocol. We measured the induction of Flk-1 (also known as *Kdr*) and Pdgfra, receptor tyrosine kinases expressed on cardiogenic mesodermal cells (Kattman et al., 2011). Whereas control cultures showed robust induction of Pdgfra by flow cytometry, *Brg1*-deleted cultures showed a clear reduction in the number of Pdgfra- and Flk1-expressing cells (n=3; Fig. 2A). Similarly, *Brg1*-deleted cultures showed reduced expression of the mesodermal marker *Mesp1* (Fig. 2B). The remaining expression still observed for Pdgfra, Flk-1 and *Mesp1* in these experiments might be the result of residual Brg1 activity, as mesoderm is induced concomitant with addition of 4-OHT, leading to a gradual loss of Brg1 protein during mesoderm induction. Taken together, these data

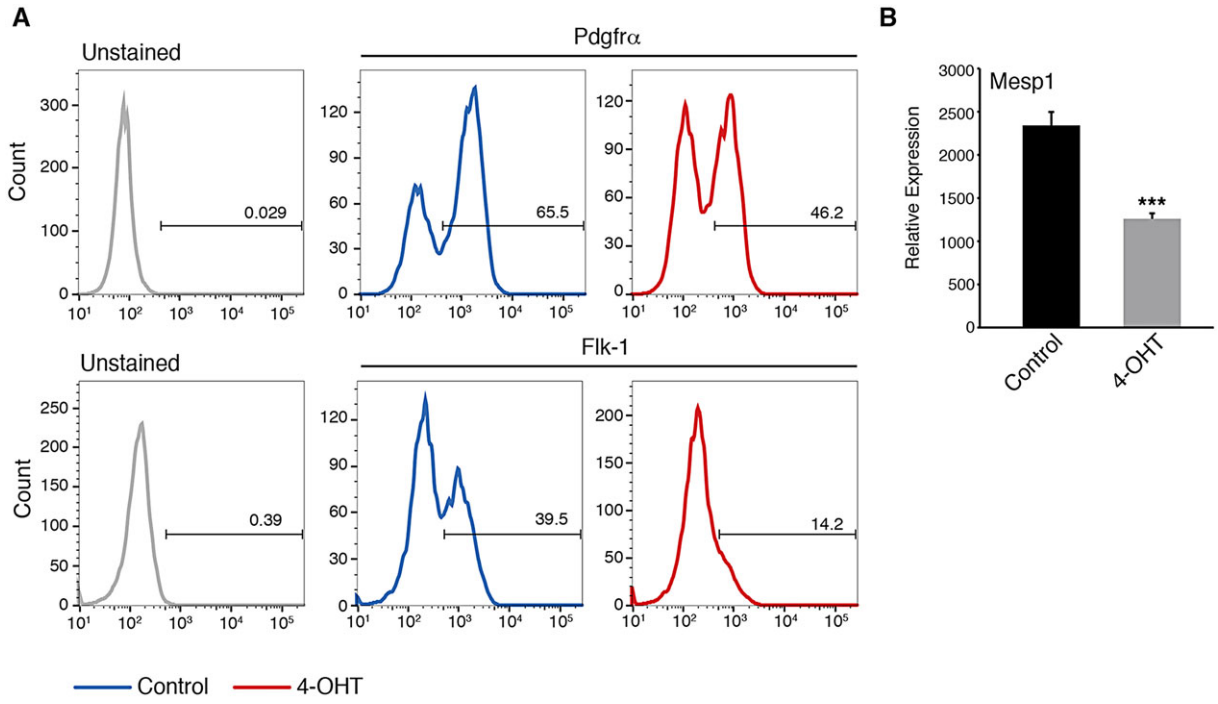

Fig. 2. Brg1 is required for robust induction of mesodermal markers. (A) Flow cytometry for Pdgfra and Flk-1 at day 4 of differentiation demonstrates a lower percentage of cells expressing these mesoderm markers in cultures deleted for *Brg1*. (B) Quantitative PCR demonstrates reduced expression of *Mesp1* in day 4 cultures depleted for *Brg1*. ***P<0.001; Student's t-test.

Development (2015) 142, 1418-1430 doi:10.1242/dev.109496

demonstrate that *Brg1* is required in ESCs for robust induction of molecular markers of mesoderm.

Brg1 is required for gene activation and maintenance of gene repression during mesoderm differentiation

To identify the *Brg1*-dependent transcriptional program during mesoderm differentiation, we collected cultures before mesoderm induction (day 2) and cultures 40 h after treatment with Vegf, activin A and Bmp4 (day 4) that had been treated with either 4-OHT or control, and measured global gene expression by RNA-seq (Fig. 3A). This allowed identification of the transcriptional changes that occur normally during mesoderm differentiation, in addition to genes differentially expressed between 4-OHT and control. In this way, we could determine whether *Brg1*-dependent genes demonstrate a common expression pattern during mesoderm induction. Using stringent criteria (FDR=1%, fold change ≥2), we identified 350 downregulated and 502 upregulated genes in *Brg1*-deleted cultures (Fig. 3B; supplementary material Table S2). This analysis demonstrated that *Brg1* was downregulated more than tenfold in *Brg1*-deleted cultures, confirming the efficacy of the genetic deletion. Among the downregulated genes were *Flk1* and *Mesp1*, mesodermal markers that demonstrated reduced induction by flow cytometry or quantitative PCR. We also found other genes essential for mesoderm development, of which the expression was reduced by loss of *Brg1*, including *Cxcr4*, *Cyp26a1* and *Snai1*. *Cxcr4* is expressed in Flk-1/Pdgfra-expressing mesoderm and mediates differentiation towards the cardiac lineage. *Cyp26a1* modulates retinoic acid signaling, a crucial regulator of mesodermal patterning (Aulehla and Pourquié, 2010; Chiriac et al., 2010; Nelson et al., 2008). *Snai1* is a transcriptional repressor that controls epithelial-to-mesenchymal transition (EMT) and mesoderm morphology *in vivo* (Carver et al., 2001). Gene ontology (GO) analysis revealed that downregulated genes were enriched for genes involved in cell adhesion as well as those associated broadly with development (multicellular organismal process) and signaling (molecular transducer activity) (Table 2; supplementary material Table S3). These findings are consistent with defective induction of mesodermal genes in *Brg1*-deficient cultures. *Pdgfra*, which had reduced expression, as measured by flow cytometry (Fig. 2A), was downregulated 1.93-fold in our RNA-seq analysis and thus fell slightly below our stringent criteria for significance. Therefore, our statistical cutoff is probably a conservative estimate of *Brg1*-dependent gene expression.

Examination of the genes upregulated by loss of *Brg1* (Fig. 3B) revealed Wnt signaling ligands (*Wnt8a*, *Wnt9a*, *Wnt7b*, *Wnt4*, *Wnt10a* and *Wnt6*), Wnt antagonists (*Sfrp1* and *Frzb*), and numerous developmental transcription factors (TFs). The latter included TFs from the Fox, Tbx, Mef2, Dlx, Runx, Pax, Lhx, Six, Nkx, Sox, Pou, Cdx, Irx and Hox TF families. GO analysis was consistent with this finding; upregulated genes demonstrated strong enrichment for genes associated with development, morphogenesis and transcription factor function (Table 2). Investigation of expression data from a broad range of murine tissues and cell types confirmed that upregulated TFs are expressed in many distinct and non-overlapping lineages (supplementary material Fig. S2), demonstrating that loss of *Brg1* does not result in differentiation of ESCs towards a single, non-mesodermal lineage. Strikingly, many (18 of 38) *Hox* genes, representing all four *Hox* clusters, were upregulated in *Brg1*-deleted mesoderm.

Within genes significantly upregulated by loss of *Brg1* were numerous TFs that function during heart development, despite the striking defect for these cultures to generate cardiomyocytes at subsequent stages. This group included the well-characterized regulators of skeletal and cardiac myogenesis *Myocd* and *Mef2b* as well as conserved cardiogenic factors *Tbx5* and *Nkx2-5*. Of particular note was *Nkx2-5*, the expression of which increased more than sevenfold in *Brg1*-deficient mesoderm. Our previous studies (Wamstad et al., 2012) have shown that these factors are expressed at low levels in mesodermal cultures, becoming robustly expressed only later, concomitant with the onset of cardiomyocyte differentiation. We did not observe broad upregulation of markers of cardiomyocytes in these cultures, suggesting instead that the

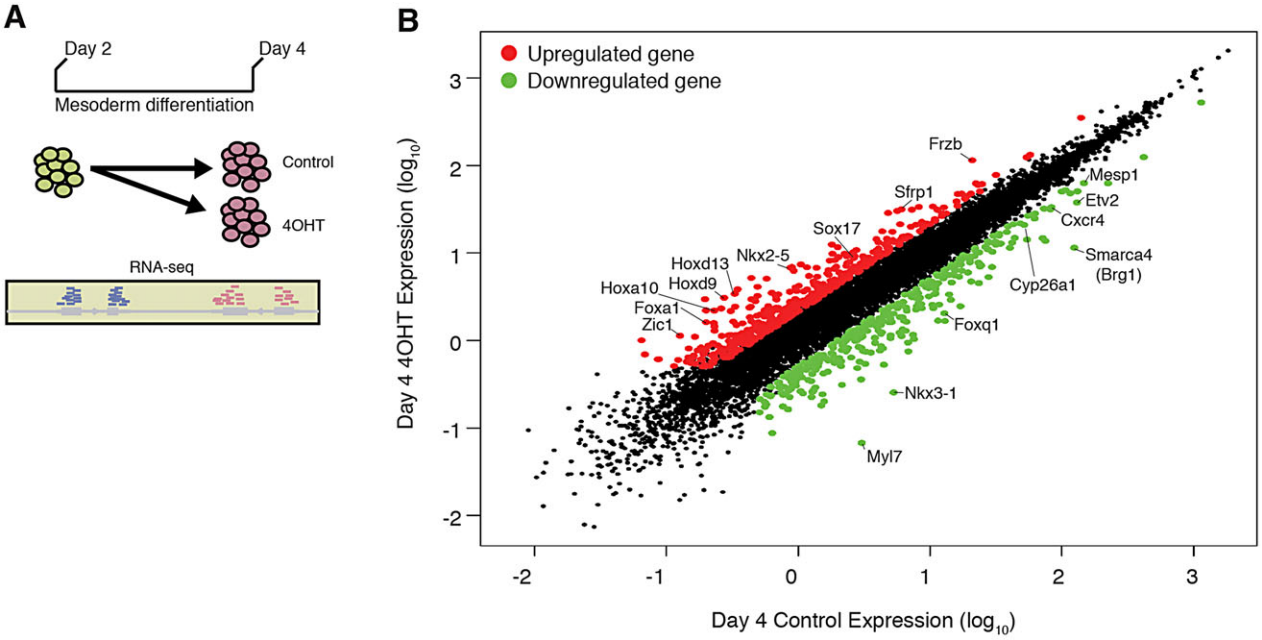

Fig. 3. Global expression analysis of *Brg1*-deleted mesodermal cultures reveals dysregulation of essential developmental genes. (A) Cartoon of the RNA-seq experimental design. (B) Day 4 expression in control samples plotted versus day 4 expression in 4-OHT-treated samples. Genes significantly changed (>twofold change, FDR=1%) are colored in red and green for upregulated and downregulated, respectively. Example genes are highlighted.

Development (2015) 142, 1418-1430 doi:10.1242/dev.109496

Table 2. Gene ontology analysis of genes significantly downregulated or upregulated by loss of *Brg1*

Downregulated genes	Upregulated genes
Biological process (*z*-score, adjusted *P*-value)	**Biological process (*z*-score, adjusted *P*-value)**
Cell adhesion (10.35, *P*=0.034)	Anatomical structure development (13.14, *P*=0.021)
Multicellular organismal process (8.22, *P*=0.034)	Regionalization (12.17, *P*=0.021)
Regulation of chronic inflammatory response (7.79, *P*=0.034)	Anatomical structure morphogenesis (11.92, *P*=0.021)
Regulation of multicellular organismal process (7.26, *P*=0.034)	Multicellular organismal process (11.08, *P*=0.021)
Taxis (7.22, *P*=0.034)	Cellular developmental process (9.82, *P*=0.021)
Molecular function (*z*-score, adjusted *P*-value)	**Molecular function (*z*-score, adjusted *P*-value)**
Extracellular matrix structural constituent (11.50, *P*=0.034)	Sequence-specific DNA binding (12.60, *P*=0.021)
Calcium ion binding (8.78, *P*=0.034)	Sequence-specific DNA binding transcription factor activity (12.29, *P*=0.021)
Pattern binding (8.65, *P*=0.034)	TAP binding (8.55, *P*=0.021)
Molecular transducer activity (7.33, *P*=0.034)	Acetylcholine-activity cation-selective channel activity (7.90, *P*=0.021)
Collagen binding (6.46, *P*=0.034)	Sodium channel activity (6.11, *P*=0.021)

upregulation of these cardiogenic TFs reflects the broader misexpression of inappropriate developmental regulators in *Brg1*-deficient mesodermal cultures.

Brg1 might function to facilitate dynamic changes in gene expression that occur during mesoderm induction or might be required to maintain active and repressed transcriptional states. To better understand the function of *Brg1* in transcriptional regulation of mesoderm differentiation, we investigated the expression patterns of *Brg1*-dependent genes during this process. We rank-ordered genes based on fold change in gene expression during normal mesoderm differentiation (day 4 control versus day 2) and compared normal and *Brg1*-deleted mesoderm differentiation. We limited our analysis to only those genes measured by RNA-seq in all three experimental conditions. We found that the majority (82%) of genes downregulated by loss of *Brg1* are activated during normal mesoderm induction (Fig. 4A, left bar); *Brg1* deletion during mesoderm induction led to less robust activation for these genes (Fig. 4A, right bar). By contrast, genes upregulated by loss of *Brg1* showed a tendency for repression during normal mesoderm differentiation. We found that upregulated genes were generally expressed at very low levels in normal mesodermal cultures (supplementary material Fig. S3). Loss of *Brg1* leads to derepression of these genes during mesoderm differentiation. Collectively, our global gene expression analysis supports broad roles for *Brg1* in gene activation and maintaining gene repression of key developmental regulators during mesoderm differentiation of ESCs.

We next investigated to what extent *Brg1* is required for transcriptional change during mesoderm induction. We identified genes differentially expressed between day 4 control and day 2 (FDR=1%, fold change ≥2), categorized these genes as either activated or repressed during mesoderm induction, and overlapped these gene sets with *Brg1*-dependent genes. This analysis revealed that 18% of genes activated during normal mesoderm differentiation (i.e. significantly higher expression at day 4) had reduced expression in *Brg1*-deleted mesodermal cultures, compared with just 2% of repressed genes. Mesoderm-activated genes were considerably enriched for those dependent on *Brg1* for expression (Fig. 4B). This demonstrates that a substantial proportion of the mesoderm transcriptional program requires *Brg1* for proper activation.

Brg1 is required for H3K27ac enrichment at dynamically activated enhancers proximal to dysregulated genes

To better understand the mechanism by which *Brg1* affects the mesodermal transcriptional program, we defined the genomic regions bound by Brg1 in mesodermal cultures. To this end, we used ESCs harboring a *Brg1* allele that encodes a 3×-FLAG epitope tag fused to the C-terminal end of Brg1 targeted to the endogenous *Brg1* locus (Attanasio et al., 2014). We confirmed the expression of Brg1-FLAG in cultured pluripotent ESCs (supplementary material Fig. S4). Purification of Brg1-FLAG using an anti-Flag column yielded a staining pattern that closely resembled those published for BAF complexes (Ho et al., 2009; Wang et al., 1996) (supplementary material Fig. S4), consistent with Brg1-FLAG incorporation into BAF complexes. Mass spectrometry of isolated complexes revealed a composition highly similar to previously reported esBAF complexes (Ho et al., 2009) (data not shown). Mice homozygous for the Brg1-FLAG allele are viable, further indicating that the allele is fully functional, and ChIP-seq data, obtained in mouse tissues using this Brg1-FLAG allele, strongly correlated with published Brg1 ChIP-seq data obtained with antisera (Attanasio et al., 2014). We differentiated Brg1-FLAG ESCs to mesodermal precursors and performed chromatin immunoprecipitation and deep sequencing (ChIP-seq) on biological duplicate samples. FLAG ChIP-seq replicates overlapping H3K27ac-enriched regions were well correlated (r^2=0.71) and showed modest enrichment that probably reflects the transient and dynamic nature of chromatin remodeler binding. To identify high-confidence Brg1-bound regions from these data, we overlapped statistically enriched peaks identified through an input-corrected Poissonian model across both replicates (Marson et al., 2008) and identified 3027 bound regions distributed throughout the mouse genome (see supplementary material Methods, Table S4). Given the modest enrichment of our FLAG ChIP-seq dataset, we expect these regions, statistically enriched in both biological replicates, to represent a conservative estimate of Brg1 occupancy.

To validate Brg1-FLAG-bound regions, we performed ChIP-exo, using an antibody against endogenous Brg1 (Morris et al., 2014) in Brg1-FLAG ESCs differentiated to mesodermal precursors in biological duplicates. As expected, our 3027 Brg1-FLAG-bound regions demonstrated modest but clear enrichment for Brg1 in the ChIP-exo dataset (Fig. 5A), with occupancy characteristics similar to published results (Morris et al., 2014; Shi et al., 2013). Correlation between anti-FLAG and anti-Brg1 ChIP over H3K27ac-enriched regions is 0.52. To further validate these regions and the specificity of the antibody, we performed Brg1 ChIP-exo on differentiating *Brg1*$^{f/f}$;*Actin-CreER* ESCs treated with either THF (control) or 4-OHT (deletion of *Brg1*) for 48 h. Brg1 enrichment, modest but clear in THF-treated samples, was greatly reduced in *Brg1*$^{f/f}$;*Actin-CreER* ESCs treated with 4-OHT. Taken together, we have defined Brg1-bound regions consistently enriched by different methods, which are sensitive to genetic deletion of Brg1. We acknowledge that the modest enrichment only allows the identification of high-confidence high-enrichment regions; therefore, our conclusions regarding the direct function of Brg1 are limited to these regions.

Development (2015) 142, 1418-1430 doi:10.1242/dev.109496

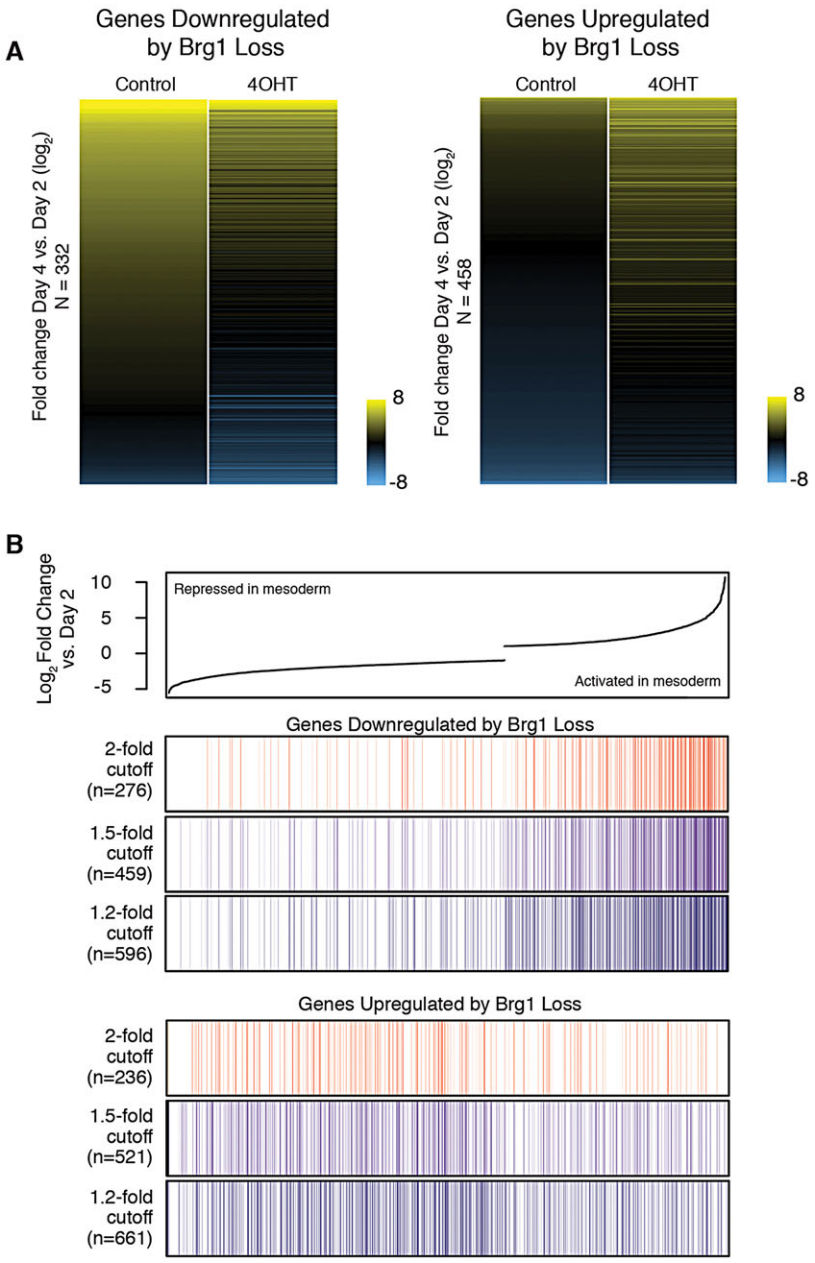

Fig. 4. *Brg1* is required for gene activation and maintenance of gene silencing during mesoderm differentiation. (A) Heat map of $\log_2$-fold change in expression during mesoderm differentiation for genes significantly downregulated or upregulated by loss of *Brg1*. (B) (Top) Genes are rank-ordered based on $\log_2$-fold change in expression between day 4 control and day 2 (normal mesoderm differentiation). Only genes significantly changed during mesoderm differentiation are shown. (Bottom) Color bars depict distribution of genes downregulated by loss of *Brg1* by numerous fold change cut-offs. Colors vary only for ease of visualization and do not correlate to numerical values. Each vertical line represents a single dysregulated gene. Genes downregulated by loss of *Brg1* cluster to the right, suggesting a role for *Brg1* in gene activation during mesoderm differentiation. Conversely, genes upregulated by loss of *Brg1* are more often found repressed during mesoderm differentiation. *N* indicates the number of *Brg1*-dependent genes shown.

Comparison of Brg1-bound regions with genomic annotations revealed Brg1 binding within gene promoters, introns, exons and intergenic regions (Fig. 5B). We identified 691 genes with reproducible binding of Brg1 within 2.5 kb of the transcriptional start site. Some genes in this group were also significantly changed in our RNA-seq dataset. However, an intersection of Brg1-bound promoters with *Brg1*-dependent genes revealed little overlap (Fig. 5C), as observed for other chromatin remodelers (Gelbart et al., 2005; Sala et al., 2011). We find the majority of genes with Brg1 promoter enrichment do not show significant changes in gene expression. Moreover, most *Brg1*-dependent genes lacked robust Brg1 binding within the promoter. This suggests that Brg1 does not predominately modulate gene expression through promoter regulation in differentiating mesoderm.

Brg1 localizes to well-characterized enhancers (Bultman et al., 2005) and predicted enhancers genome-wide (Euskirchen et al., 2011; Hu et al., 2011; Rada-Iglesias et al., 2011; Yu et al., 2013). Given that only 23% of Brg1 peaks were found within promoter regions, we hypothesized that Brg1 functions at distal enhancers. To test this, we generated genome-wide maps of H3K27ac in control and 4-OHT-treated mesodermal cultures in biological duplicates. H3K27ac marks active enhancers and can be used to identify putative distal regulatory elements genome-wide (Calo and Wysocka, 2013). Comparison of Brg1-FLAG and H3K27ac ChIP-seq signals at Brg1-enriched loci showed substantial enrichment for H3K27ac at Brg1-bound regions (Fig. 5A; see also Attanasio et al., 2014). Moreover, our ChIP-seq data revealed a high correlation between Brg1 and H3K27ac signals throughout the genome (Fig. 5D; supplementary material Fig. S5). Using our genome-wide maps of H3K27ac, we identified 16,724 putative enhancer regions distal (>2.5 kb) from the transcriptional start site. Strikingly, we found that 68% of Brg1-bound regions distal to transcriptional start sites overlapped with predicted enhancer regions (P<0.0001; 10,000 permutations). Thus, Brg1 associates with a proportion of H3K27ac-marked enhancers genome-wide in mesodermal cultures.

Development (2015) 142, 1418-1430 doi:10.1242/dev.109496

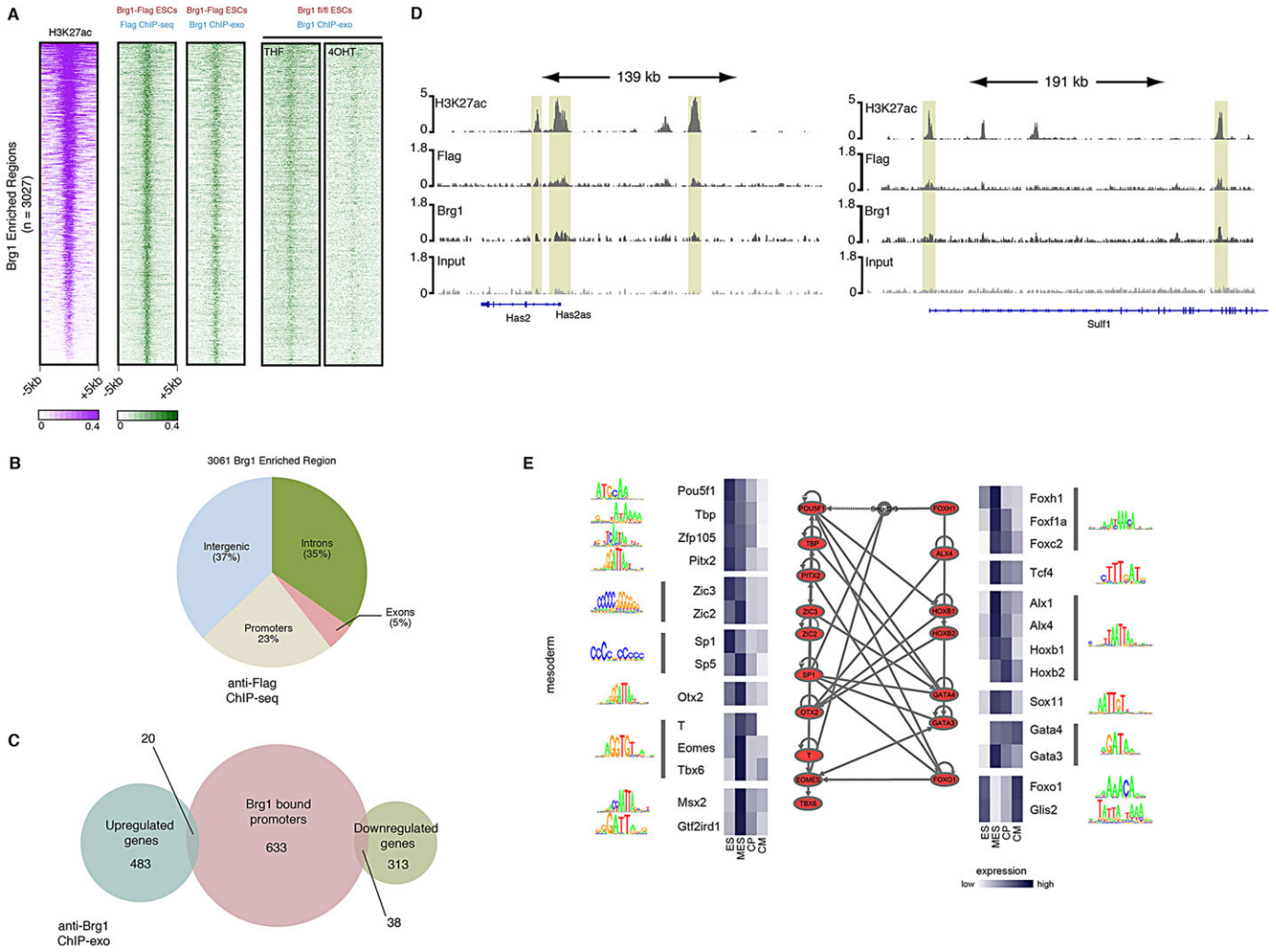

Fig. 5. *Brg1* co-localizes with H3K27ac genome-wide. (A) Density of ChIP-seq reads for H3K27ac, anti-FLAG ChIP-seq and anti-Brg1 ChIP-exo in Brg1-FLAG ESCs, and anti-Brg1 ChIP-exo in THF- and 4-OHT-treated *Brg1*$^{fl/fl}$ ESCs. Plots show ±5 kb around the midpoint of each Brg1-enriched region ranked according to H3K27ac density, and demonstrate significant co-localization of Brg1 with H3K27ac. Brg1 is detected at these regions across distinct cell lines and ChIP antibodies, and is lost upon genetic deletion. (B) Distribution of Brg1-enriched regions across the mouse genome. (C) Overlap between genes with Brg1 enrichment within 2.5 kb of the TSS and genes dysregulated by loss of *Brg1* demonstrates little overlap between *Brg1*-dependent genes and Brg1-bound promoters. (D) Co-localization of Brg1 and H3K27ac at example genomic regions. *y*-axis shows reads per bin per million. (E) Motifs enriched at Brg1-occupied enhancer elements. TRANSFAC positional Weight Matrices for each significantly ($q<0.001$) enriched motif is shown next to transcription factors known to bind these motifs that are expressed at the mesoderm stage (interquartile range-normalized RPKM values are shown). Known regulatory interactions, as identified using the Ingenuity Pathway analysis, are also annotated for each gene.

We searched Brg1-bound enhancers for enriched transcription factor DNA binding motifs that might predict a mechanism for site-specific recruitment of Brg1. H3K27ac^{+} Brg1-bound regions were scanned using the 'match' algorithm of TRANSFAC. A number of motifs were significantly enriched ($q<0.001$), with many belonging to well-known regulators of mesodermal differentiation, including T-box, GATA and Fox factors, which function in a highly interactive network (Fig. 5E). Although enrichments were highly significant, fold enrichment in motif abundance between Brg1-associated enhancers and all enhancers was modest (between 1.11- and 1.95-fold enrichment). We conclude that Brg1-bound enhancers are enriched for specific developmental TFs, but it is unlikely that these factors alone direct Brg1 occupancy, and might instead reflect bias in Brg1 recruitment to developmentally regulated enhancers.

The presence of Brg1 at enhancers suggests that Brg1 regulates transcriptional activation during mesoderm induction through modulation of enhancer activity. We therefore asked whether H3K27ac levels were altered in *Brg1*-deleted mesodermal cultures. To this end, we compared H3K27ac genome-wide maps from control and 4-OHT-treated mesodermal cultures, and rank-ordered promoter and enhancer regions based on fold change in H3K27ac in *Brg1*-deleted cultures. We found that levels of H3K27ac were largely unchanged at promoter regions (median $\log_2$-fold change=0.07), although downregulated genes showed clear reductions in H3K27ac levels proximal to the TSS, probably reflecting decreased transcriptional activity at these genes (supplementary material Fig. S6). In contrast to promoter regions, we observed a global reduction in H3K27ac levels at predicted enhancer regions in *Brg1*-deleted cultures (median $\log_2$-fold change=−0.39) (Fig. 6A). Consistent with a functional role for enhancer activity in the transcriptional changes seen in *Brg1*-deleted cultures, we observed a correlation between changes in H3K27ac seen at an enhancer and changes in expression of its nearest gene

Development (2015) 142, 1418-1430 doi:10.1242/dev.109496

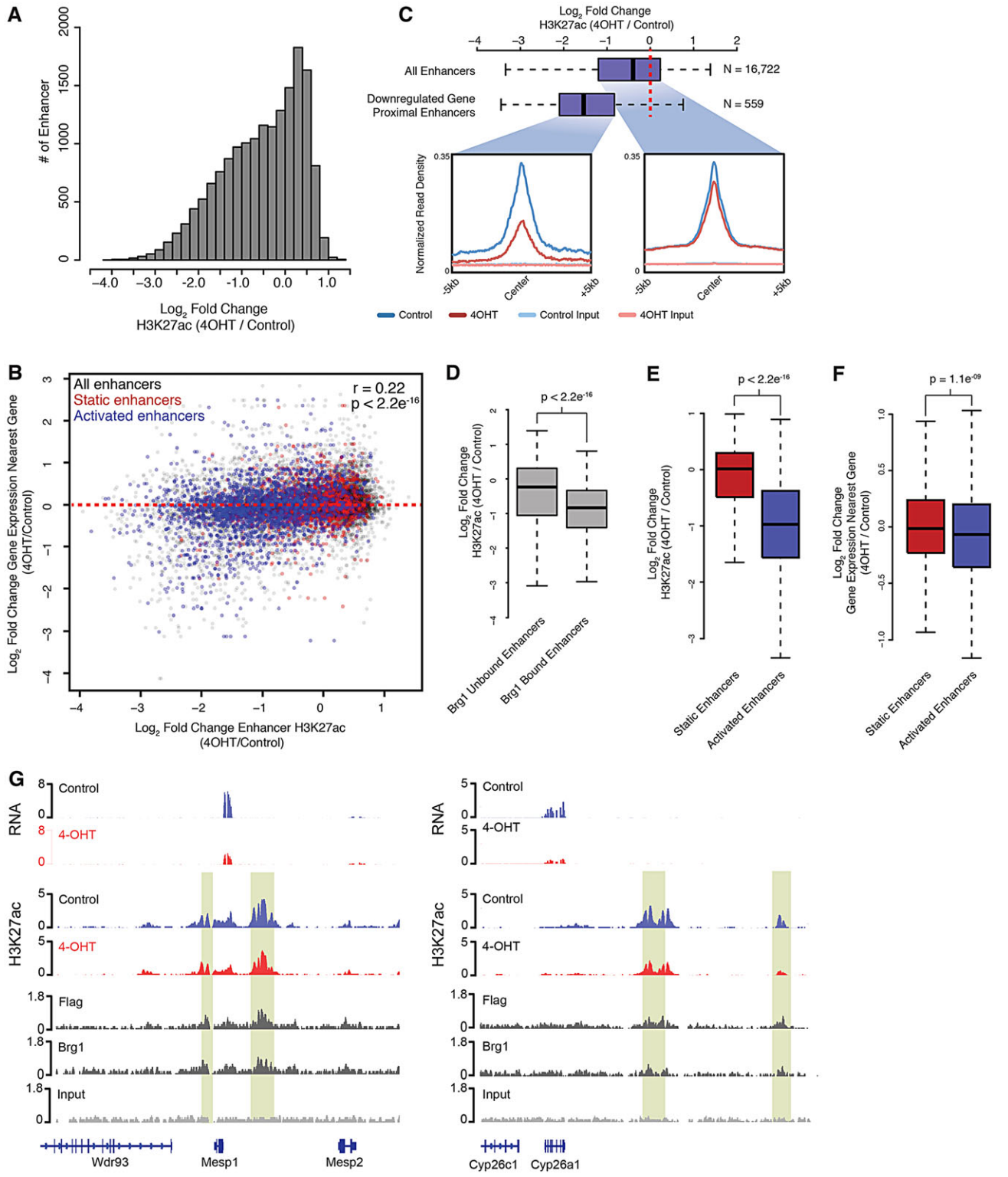

Fig. 6. *Brg1* is required for enhancer activation in differentiating mesodermal cultures. (A) Histogram of $\log_2$-fold change in H3K27ac at predicted enhancers. (B) Scatterplot of $\log_2$-fold change of H3K27ac at predicted enhancers and the $\log_2$-fold change in gene expression between day 4 4-OHT and day 4 control cultures of the nearest gene to each enhancer plotted. Red and blue dots highlight enhancers marked by H3K27ac in undifferentiated ESCs and mesodermal cultures (static enhancers), and those marked in mesoderm cultures only (activated enhancers), respectively. (C) Box plots of $\log_2$-fold change of subsets of predicted enhancers with read density profiles of each enhancer cohort. Enhancers associated with downregulated genes include enhancers of which the most proximal gene is significantly downregulated in *Brg1*-deleted mesoderm. Downregulated gene-associated enhancers show greater average loss in H3K27ac than all enhancers. (D) Box plots of $\log_2$-fold change in H3K27ac for predicted enhancers in *Brg1*-deficient cultures. Enhancers are separated into Brg1-bound and unbound cohorts based on the presence or absence of a Brg1-enriched region, respectively. (E,F) Box plots of $\log_2$-fold change in H3K27ac (E) or expression of the nearest gene (F) for static and activated enhancers in *Brg1*-deficient cultures. (G) H3K27ac at putative enhancer regions proximal to the *Mesp1* and *Cyp26a1* genes. *y*-axis shows reads per bin per million.

Development (2015) 142, 1418-1430 doi:10.1242/dev.109496

(Fig. 6B). This relationship was observed despite limitations of computational approaches in predicting enhancer-gene regulatory pairs. Furthermore, we found that enhancers proximal to significantly downregulated genes showed greater reductions in H3K27ac compared with all putative enhancers (Fig. 6C). These findings support a functional role for *Brg1*-dependent enhancer activity in the transcriptional control of mesoderm differentiation.

To investigate whether Brg1 regulates enhancer activity directly through its recruitment to these loci, we partitioned mesodermal enhancers into Brg1-bound or Brg1-unbound cohorts. We found that Brg1-bound enhancers showed greater losses in H3K27ac than those without Brg1-enrichment, providing evidence that Brg1 directly modulates H3K27ac at enhancers (Fig. 6D). We also observed greater occurrence of Brg1-bound enhancers proximal to significantly downregulated genes than expected by chance alone (P=0.0002, hypergeometric test). A potential indirect role for *Brg1* in enhancer regulation through transcriptional control of histone modifying enzymes was discounted, as expression of histone acetyltransferases responsible for depositing H3K27ac at enhancers was not affected by loss of *Brg1* (supplementary material Fig. S7). These data support a direct role for *Brg1* in control of enhancer activity.

Enhancer usage is highly cell-type specific and dynamic during cell differentiation, and H3K27ac enrichment distinguishes active enhancers from other enhancer states (Calo and Wysocka, 2013). Given the requirement for *Brg1* for H3K27ac levels at enhancers proximal to downregulated genes and that many of these genes are induced during mesoderm differentiation (Fig. 4A), we hypothesized that *Brg1* might be required to activate quiescent enhancers during mesoderm differentiation. To test this, we used our published enhancer predictions in directed cardiac differentiations of ESCs to distinguish enhancers that are dynamically activated during mesoderm differentiation from those that remain active from undifferentiated cell states (Wamstad et al., 2012). We overlapped our 16,725 predicted enhancers with those identified at an analogous stage of ESC differentiation and divided this cohort into 'activated' or 'static' enhancers, based on whether these regions were uniquely marked by H3K27ac in mesodermal cultures or marked in both mesodermal cultures and ESCs, respectively. As expected, genes proximal (nearest gene) to activated enhancers are transcriptionally activated during mesoderm induction (data not shown). Whereas static enhancers showed no changes in H3K27ac on average (median $\log_2$-fold change=0.012), activated enhancers had reduced H3K27ac in *Brg1*-deleted mesoderm (median $\log_2$ fold change=−1.02) (Fig. 6B,E). Genes proximal to activated enhancers showed greater reductions in gene expression upon loss of *Brg1* than those proximal to static enhancers (Fig. 6F). Moreover, we found that activated enhancers were significantly enriched for Brg1 occupancy compared with static enhancers (Chi-squared test, P=3.043e^{-11}). Thus, our data reveal that Brg1 activity is most important at regulatory regions that are transitioning in activation status.

Consistent with a role for *Brg1* in activation of mesodermal enhancers, we found multiple Brg1-bound enhancers near the mesodermal genes *Flk1* and *Cyp26a1* that showed marked loss of H3K27ac in *Brg1*-deleted mesoderm (Fig. 6G; supplementary material Fig. S5). This included an experimentally validated regulatory region ∼30 kb upstream of the *Flk1* TSS that directs early mesodermal expression in the mouse embryo (Ishitobi et al., 2011). Furthermore, we detected a clear reduction in H3K27ac within a Brg1-bound region roughly 5 kb upstream of the *Mesp1* TSS, which functions as a regulatory enhancer for *Mesp1* expression (Haraguchi et al., 2001) (Fig. 6G). These enhancers are not marked by H3K27ac in ESCs and, thus, are activated during mesoderm differentiation to coordinate the transcriptional activation of nearby genes. We propose that *Brg1* regulates the transcriptional induction of mesodermal gene expression through binding to distal regulatory regions and facilitating the recruitment of these regions towards the activation of nearby genes.

Finally, Brg1 has been observed to associate with large enhancer collectives that have been dubbed 'super' or 'stretch' enhancers (Hnisz et al., 2013; Parker et al., 2013; Whyte et al., 2013). Based on correlation with transcriptional activity, these large stretches of H3K27ac have been proposed to be associated with highly cell type-specific gene regulation. We identified 4894 'super-enhancers', of which 594 were bound by Brg1. Although these had significant reductions in H3K27ac occupancy in the absence of Brg1, the loss of H3K27ac was significantly less pronounced than smaller dynamic enhancers (supplementary material Fig. S6). Thus, Brg1 is important for activating initially silent enhancers and is less important at larger enhancers, perhaps due to redundant mechanisms of enhancer activation (Hnisz et al., 2013).

Brg1 is required for H3K27me3 at developmental regulators in mesodermal cultures

We next investigated the mechanism by which *Brg1* regulates the repression of developmental regulators in *Brg1*-deleted mesoderm. Intersection of our RNA-seq analysis with published ChIP-seq datasets of H3K27me3 and Polycomb subunit occupancy in undifferentiated ESCs demonstrated that upregulated genes were highly enriched for Polycomb targets (Ku et al., 2008) (supplementary material Fig. S8). Given that *Brg1* positively regulates PRC2 repression of *Hox* loci in undifferentiated ESCs (Ho et al., 2011), we hypothesized that *Brg1* is broadly required for PRC2-mediated silencing in differentiating mesoderm.

To test this, we measured genome-wide occupancy of H3K27me3 in control and 4-OHT-treated mesodermal cultures by ChIP-seq in biological triplicate. We analyzed the enrichment of H3K27me3 at the promoters of genes upregulated by loss of *Brg*1 in normal mesodermal cultures and found that a subset of these genes (termed group I) were substantially enriched for H3K27me3 (Fig. 7A). This subset included nearly all derepressed developmental TFs. In agreement with the exclusivity of the two marks, group I genes were relatively low in H3K27ac, which instead marked a second subset of upregulated genes with few developmental regulators (group II).

We focused on group I genes and compared H3K27me3 genome-wide maps from control and 4-OHT-treated mesodermal cultures, to determine whether loss of *Brg1* led to reduced levels of H3K27me3. Whereas most developmental TFs were still marked by H3K27me3 in Brg1-depleted cultures, we observed clear, reproducible reductions in H3K27me3 at group I genes (Fig. 7B,C; supplementary material Fig. S5C). Clear examples of this are *Irx1* and *Nkx2-5*, two homeodomain TFs that are upregulated upon loss of *Brg1* (Fig. 7B). We did not observe reduced expression of PRC2 subunits or H3K27 demethylases in our RNA-seq analysis, arguing against an indirect effect on H3K27me3 levels through *Brg1* transcriptional regulation of these chromatin regulators (supplementary material Fig. S7). We next considered that reduced levels of H3K27me3 might result from abrogated recruitment of PRC2 or reduced activity of recruited complexes. To distinguish between these two possibilities, we measured genome-wide occupancy of Suz12, an essential subunit of PRC2 complexes (Surface et al., 2010), in control and 4-OHT-treated mesodermal cultures in biological duplicate. Suz12 demonstrated

Development (2015) 142, 1418-1430 doi:10.1242/dev.109496

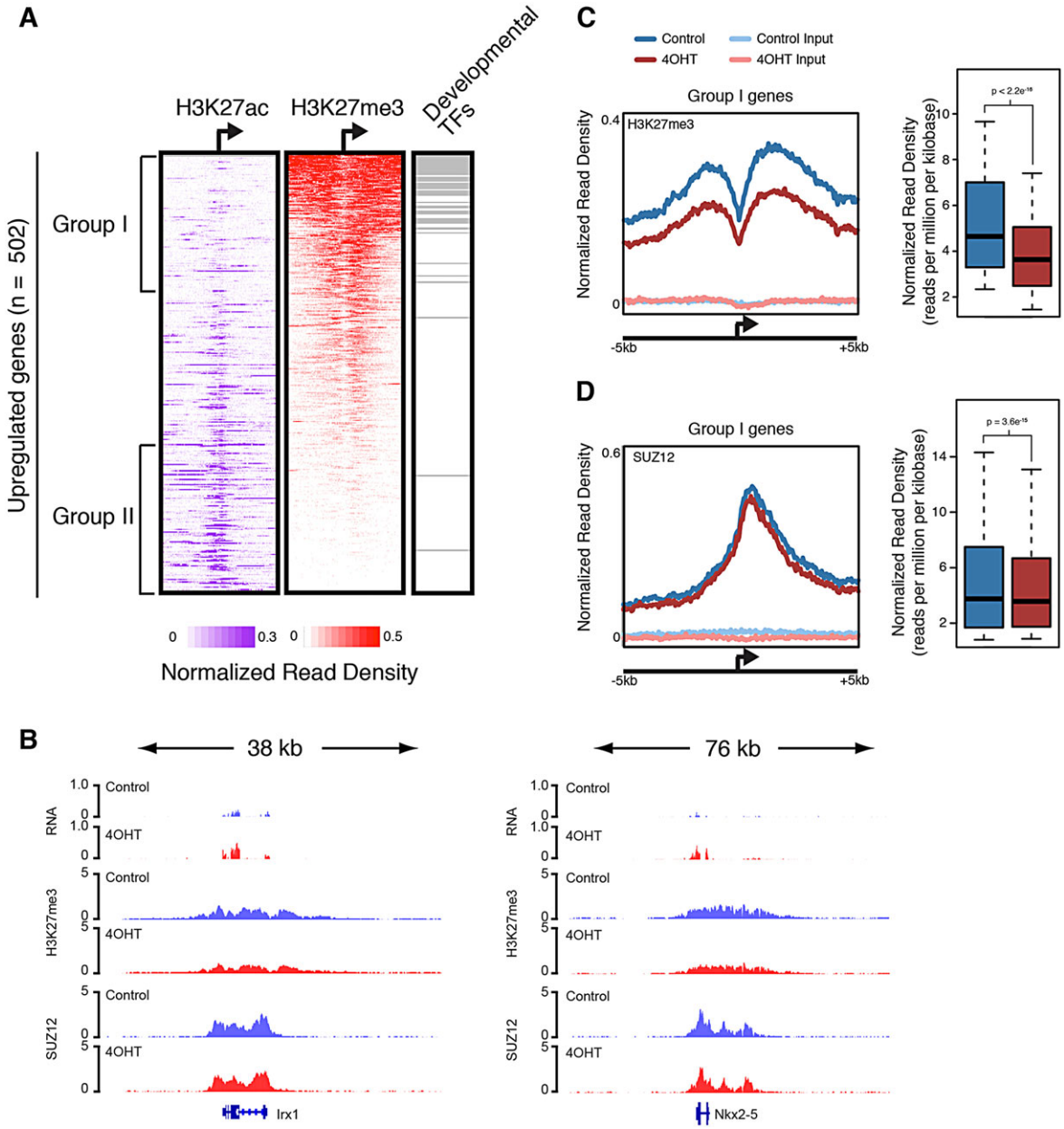

Fig. 7. *Brg1* is required for H3K27me3 levels at derepressed developmental regulators. (A) Density of ChIP-seq reads for H3K27ac and H3K27me3±5 kb of the TSS of upregulated genes. Regions are ranked according to H3K27me3 density. Right bar indicates distribution of developmental transcription factors (TFs). Most developmental TFs are marked by H3K27me3 and not by H3K27ac. (B) Example genomic regions with loss of H3K27me3 at derepressed genes. *y*-axis denotes reads per bin per million. (C,D) (Left) Average ChIP-seq or input signal from control or 4-OHT-treated cultures at promoters of group I genes for (C) H3K27me3 or (D) Suz12. (Right) Box plot of normalized (C) H3K27me3 or (D) Suz12 ChIPseq read density at group I gene promoters (±5 kb of TSS) for day 4 control (blue) or day 4 4-OHT (red). Significance between groups was determined using a two-sided paired Mann–Whitney *U*-test.

clear enrichment at group I genes in both normal and *Brg1*-deleted cultures. Composite analysis of all group I genes revealed a modest, albeit statistically significant, reduction in Suz12 occupancy (Fig. 7D); however, this reduction was small in comparison to the reduction in H3K27me3. Thus, Brg1 probably modulates PRC2 repression independently of PRC2 recruitment.

DISCUSSION

Our findings support a role for *Brg1* in balancing lineage-specific gene expression (summarized in Fig. 8). In particular, *Brg1* is essential for transcriptional activation of essential mesodermal genes during mesoderm induction. Our genome-wide occupancy data support a primary role for *Brg1* at distal enhancers rather than at promoters. The absence of a strong correlation between Brg1 promoter occupancy and gene regulation might reflect the greater stability of chromatin states at promoter regions seen across cell-types and during differentiation (Ernst et al., 2011; Wamstad et al., 2012).

Brg1-bound loci distal to TSSs largely overlapped putative enhancer regions marked by H3K27ac, consistent with findings in other cell types (Euskirchen et al., 2011; Hu et al., 2011; Rada-Iglesias et al., 2011; Yu et al., 2013). Our data show that H3K27 acetylation depends on Brg1 at a number of loci. Of particular interest, our findings demonstrate that differentiating ESCs are most sensitive to Brg1 function at dynamic enhancer regions, pointing to an essential role for *Brg1* in the transition of developmental

Development (2015) 142, 1418-1430 doi:10.1242/dev.109496

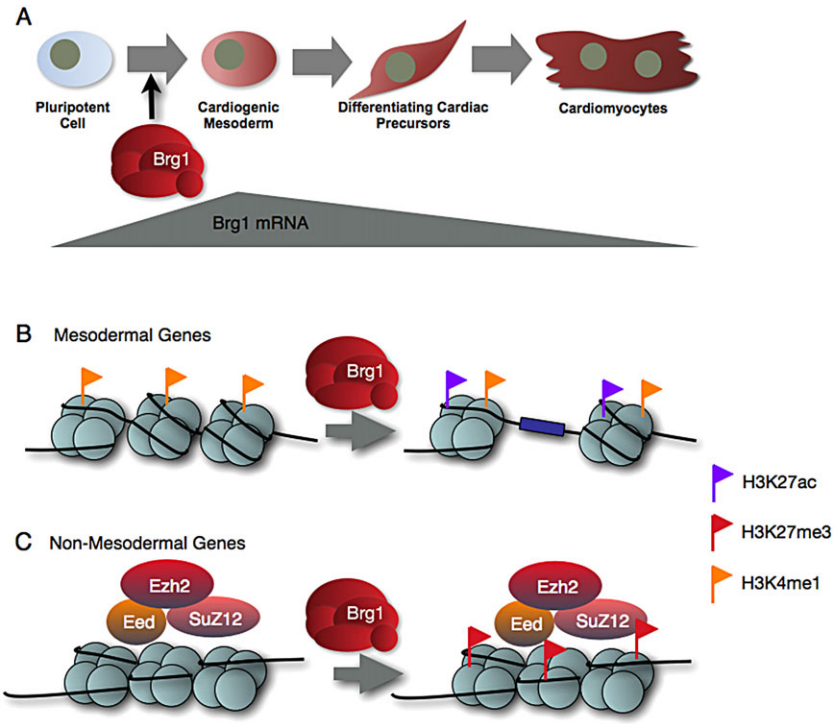

Fig. 8. Summary model. (A) Dynamic expression of Brg1 during cardiac differentiation peaks at the mesoderm stage. Brg1 function is most crucial during the mesoderm-induction stage. (B,C) Mechanisms of Brg1 function during mesoderm induction. (B) Brg1 is required for silent or poised enhancer to transition to an H3K27ac^{+} active state. (C) Brg1 is required at non-mesodermal genes to promote Polycomb complex-mediated repression.

enhancers from inactive to active. This might reflect the importance of chromatin remodeling in the conversion of inaccessible chromatin to open chromatin by facilitating TF binding and histone acetyltransferase recruitment. A similar function for BAF complexes has been proposed downstream of Cer1-mediated activation of *Nkx2-5* (Cai et al., 2013). BAF and the related yeast SWI-SNF complexes mediate TF recruitment (Hu et al., 2011; Kwon et al., 1994; Takeuchi and Bruneau, 2009), but the functional interplay between SWI-SNF family complexes and histone acetyltransferases is less clear (Agalioti et al., 2000; Narlikar et al., 2002). Our data suggest that *Brg1* enhances the function of histone acetyltransferases at transitioning enhancers, but the mechanism for this interaction is not clear. Once enhancer regions acquire characteristics of open chromatin, such as H3K27ac, they appear less dependent on *Brg1* in maintaining these characteristics. Thus, our findings predict that, whereas Brg1 might be recruited broadly to enhancer regions in many cell types, *Brg1*-dependent gene expression is likely to reflect those regions undergoing dynamic chromatin remodeling.

Brg1 is also required for repression of a diverse group of developmental regulators during mesoderm differentiation. BAF complexes have classically been annotated as Trithorax group (TrxG) complexes, which counteract Polycomb-mediated repression, based on studies in *Drosophila* (Tamkun et al., 1992). Indeed, *brm* knockdown leads to increased H3K27me3 in addition to reduced H3K27ac in flies (Tie et al., 2012). In mouse ESCs, loss of *Brg1* is linked to reduced H3K27me3 levels at *Hox* clusters, classic Polycomb targets (Ho et al., 2011). Our study demonstrates that loss of *Brg1* disrupts Polycomb repression of *Hox* clusters, as well as a broad range of other developmental regulators, during ESC differentiation. Thus, cooperativity between PRC2 and BAF complexes is not unique to the pluripotent state and is probably a crucial function for BAF complexes in lineage commitment. The nature of PRC2/BAF cooperativity is unclear. Our ChIP-seq analysis of Brg1 occupancy revealed few clear peaks within H3K27me3-marked domains, whereas Brg1 was found to co-occupy more clearly PRC2-regulated loci in developing organs, including heart (Attanasio et al., 2014). Therefore, in mesoderm Brg1 might associate with Polycomb-repressed genes in rare, transient interactions that are below our threshold for detection. Our ChIP-seq analysis revealed little change in Suz12 occupancy at derepressed genes, suggesting that *Brg1* is dispensable for Suz12 recruitment and might regulate PRC2 activity at bound loci. Nucleosome density affects PRC2 activity *in vitro* (Yuan et al., 2012). Thus, chromatin remodeling by BAF complexes could increase PRC2 efficiency by augmenting nucleosome fluidity. This model requires further exploration.

MATERIALS AND METHODS

Cardiomyocyte differentiation

Mouse ESCs were cultured in feeder-free conditions and serum containing media with leukemia inhibitory factor. Directed differentiations were performed as described previously (Wamstad et al., 2012). For Brg1 deletion, *Brg1*$^{fl/fl}$*;Actin-CreER* ESCs (Ho et al., 2009; Ho et al., 2011), cultures were treated with 200 nM 4-hydroxytamoxifen (4-OHT) diluted from a 5 mg/ml stock solution in tetrahydrofuran (THF) or with only THF for control. Additional details are provided in the supplementary material Methods.

Quantitative PCR

RNA was extracted using TRIzol and reverse transcribed using a High-Capacity cDNA Reverse Transcription kit (Applied Biosystems). Quantitative PCR was performed in technical triplicate using Taqman probes and expression was normalized to *Gapdh*. The following probes were used: *Mesp1* – Mm00801883_g1, *Gapdh* – 4352932E.

Western blotting, immunofluorescence and FACS analysis

For cell surface staining, cells were trypsinized, quenched with serum and washed in FACS buffer. Cells were stained with biotinylated anti-Flk-1 (Hybridoma Clone D218; 1:10,000) antibody, washed and stained with PE-conjugated anti-Pdgfra (eBioscience, 12-1401-81; 1:400) and APC-Streptavidin (1:200). Cells were analyzed on an LSRII flow cytometer (BD). For intracellular staining, cultures were trypsinized, fixed and stained with anti-cTnT (Thermo Scientific #MS295, Clone 13-11; 1:100) antibody, followed by secondary antibody. All steps were performed in D-PBS with 0.5% saponin and 4% FBS. Western blotting was performed using standard

Development (2015) 142, 1418-1430 doi:10.1242/dev.109496

techniques. Briefly, protein lysate was sonicated and cleared by centrifugation. Supernatant was diluted and boiled. Following electrophoresis, protein was transferred to a PVDF membrane. Membranes were incubated with desired antibody in 5% milk TBST overnight at 4°C, then washed in TBST and stained with secondary antibody. After antibody staining, membranes were washed, incubated in SuperSignal chemiluminescence substrate (Thermo Scientific) and visualized. Antibodies used were anti-Brg1 (Santa Cruz, sc-10768; 1:2000), anti-actin (Sigma, A1978; 1:2000) and anti-FLAG (Sigma, M2; 1:2000). For immunofluorescence, cultures were fixed, and, after blocking, were incubated with primary antibody at 4°C overnight. Slides were washed and incubated in secondary antibody. Slides were stained with Hoechst 33342 (10 µg/ml) in D-PBS, and immediately imaged in 50 µl D-PBS. The anti-cTnT (Thermo Scientific #MS295, Clone 13-11; 1:100) antibody was used.

RNA-seq

Total RNA was isolated from 1.5-2×10^6 cells using TRIzol reagent in biological duplicates for each experimental condition. 8 µg of total RNA was used as input material for the preparation of the RNA-Seq libraries, according to Illumina RNA Seq library kit with minor modifications. Briefly, mRNA was isolated using Dynabeads mRNA Purification Kit (Invitrogen), followed by fragmentation (Ambion) and ethanol precipitation. First- and second-strand synthesis were performed followed by end repair, A-tailing, adapter ligation and size selection on a Beckman Coulter SPRI TE nucleic acid extractor. 200-400 bp dsDNA was enriched by 13 cycles of PCR with Phusion High-Fidelity DNA Polymerase (NEB). Amplified libraries were sequenced on an Illumina HiSeq 2000.

RNA-seq analysis

Single-end 40-bp reads were aligned to the mouse genome (mm9) using Bowtie (Langmead et al., 2009). Differential gene expression between conditions was determined using the USeq package (Nix et al., 2008) considering all Refseq genes. Genes with an FDR of ≤1% and twofold expression change were considered significantly differentially expressed unless otherwise noted. USeq was also used to calculate reads per kilobase exon per million reads (RPKM) and fold change values between conditions. Mapped reads were filtered to allow a maximum of 50 identical reads, and genes expressed <0.5 RPKM in all conditions were excluded from subsequent analysis. GO analysis was performed using Go Elite (http://www.genmapp.org/go_elite/), with all genes having an RPKM >0.5 in at least one condition serving as the gene universe. Graphical representation of upregulated and downregulated genes was performed in R.

ChIP-seq/ChIP-exo

Chromatin immunoprecipitation of histone modifications were performed according to Lee et al. (2006) with minor modifications, in biological duplicate for H3K27ac, Suz12 and FLAG. H3K27me3 ChIP-seq was performed in biological triplicate. Additional details are provided in the supplementary material Methods. Antibodies used were anti-FLAG (Sigma, M2 F1804; 10 µg), anti-H3K27ac (ActiveMotif, #39134; 5 µg), anti-H3K27me3 (Millipore, 17-622; 5 µg) and anti-Suz12 (Bethyl, A302-407A; 5 µg). ChIP-seq analysis pipeline and statistical methods are provided in the supplementary material Methods.

Brg1 ChIP-exo was performed as previously described (Serandour et al., 2013) using anti-Brg1 antibody (Abcam, 110641; 3 µg). Briefly, Brg1 ChIP was performed, and, while still on magnetic beads, the immunoprecipitated DNA was polished, ligated with P7 adapter and nicks were repaired. The resulting DNA was digested with Exo I and $RecJ_f$ exonucleases (NEB). Exonuclease-digested DNA was eluted from the beads, cross-links were reversed and the bound protein was digested with proteinase K at 65°C overnight. DNA was purified using Agencourt Ampure XP beads (Beckman Coulter), denatured, and the single-stranded DNA was used to synthesize the second strand using P7 primer, followed by ligation of P5 adapter. The resulting DNA fragment was PCR-amplified, gel-purified and sequenced using an Illumina HiSeq 2500 sequencer at a minimum depth of 25 million mapped reads, with most exceeding 30 million.

Data deposition

All sequencing data have been deposited in GEO (accession number GSE45448).

Acknowledgements

We thank T. Sukonnik for immunofluorescence, J. Wylie for western blots and G. Crabtree for use of the *Brg1*$^{fl/fl}$;*Actin-CreER* ESCs. We thank P. Devine, A. Holloway and L. Boyer for input on the manuscript and G. Howard for editorial assistance.

Competing interests

The authors declare no competing or financial interests.

Author contributions

J.M.A. designed experiments, performed most of the experiments and analyses, and wrote the paper. S.K.H. performed ESC culture, isolated Brg1-FLAG complexes and performed ChIP-exo. D.H. performed ChIP-seq and ChIP-exo. S.T. performed computational analyses. L.H. generated and characterized the *Brg1*$^{fl/fl}$;*Actin-CreER* ESC line. L.A.P. provided Brg1-FLAG ESCs. B.G.B. designed experiments, directed the project and helped with writing the paper.

Funding

This work was supported by the California Institutes for Regenerative Medicine [RN2-00903], the National Heart Lung and Blood Institute (NHLBI) Bench to Bassinet Program [U01HL098179], the Lawrence J. and Florence A. DeGeorge Charitable Trust/American Heart Association Established Investigator Award (all to B.G.B.), and by William H. Younger, Jr. L.A.P. was supported by the National Institute of Dental and Craniofacial Research (NIDCR) FaceBase [grant U01DE020060NIH] and by the National Human Genome Research Institute (NHGRI) [grants R01HG003988 and U54HG006997]. L.A.P.'s research was conducted at the E.O. Lawrence Berkeley National Laboratory and was performed under Department of Energy Contract DE-AC02-05CH11231, University of California. S.K.H. was supported by postdoctoral awards from American Heart Association [13POST17290043] and Tobacco-Related Disease Research Program [22FT-0079]. Deposited in PMC for immediate release.

Supplementary material

Supplementary material available online at
http://dev.biologists.org/lookup/suppl/doi:10.1242/dev.109496/-/DC1

References

Agalioti, T., Lomvardas, S., Parekh, B., Yie, J., Maniatis, T. and Thanos, D. (2000). Ordered recruitment of chromatin modifying and general transcription factors to the IFN-beta promoter. *Cell* **103**, 667-678.

Attanasio, C., Nord, A. S., Zhu, Y., Blow, M. J., Biddie, S. C., Mendenhall, E. M., Dixon, J., Wright, C., Hosseini, R., Akiyama, J. A. et al. (2014). Tissue-specific SMARCA4 binding at active and repressed regulatory elements during embryogenesis. *Genome Res.* **24**, 920-929.

Aulehla, A. and Pourquié, O. (2010). Signaling gradients during paraxial mesoderm development. *Cold Spring Harb. Perspect. Biol.* **2**, a000869.

Bultman, S., Gebuhr, T., Yee, D., La Mantia, C., Nicholson, J., Gilliam, A., Randazzo, F., Metzger, D., Chambon, P., Crabtree, G. et al. (2000). A Brg1 null mutation in the mouse reveals functional differences among mammalian SWI/SNF complexes. *Mol. Cell* **6**, 1287-1295.

Bultman, S. J., Gebuhr, T. C. and Magnuson, T. (2005). A Brg1 mutation that uncouples ATPase activity from chromatin remodeling reveals an essential role for SWI/SNF-related complexes in beta-globin expression and erythroid development. *Genes Dev.* **19**, 2849-2861.

Cai, W., Albini, S., Wei, K., Willems, E., Guzzo, R. M., Tsuda, M., Giordani, L., Spiering, S., Kurian, L., Yeo, G. W. et al. (2013). Coordinate Nodal and BMP inhibition directs Baf60c-dependent cardiomyocyte commitment. *Genes Dev.* **27**, 2332-2344.

Calo, E. and Wysocka, J. (2013). Modification of enhancer chromatin: what, how, and why? *Mol. Cell* **49**, 825-837.

Carver, E. A., Jiang, R., Lan, Y., Oram, K. F. and Gridley, T. (2001). The mouse snail gene encodes a key regulator of the epithelial-mesenchymal transition. *Mol. Cell. Biol.* **21**, 8184-8188.

Chiriac, A., Terzic, A., Park, S., Ikeda, Y., Faustino, R. and Nelson, T. J. (2010). SDF-1-enhanced cardiogenesis requires CXCR4 induction in pluripotent stem cells. *J. Cardiovasc. Transl. Res.* **3**, 674-682.

Ernst, J., Kheradpour, P., Mikkelsen, T. S., Shoresh, N., Ward, L. D., Epstein, C. B., Zhang, X., Wang, L., Issner, R., Coyne, M. et al. (2011). Mapping and analysis of chromatin state dynamics in nine human cell types. *Nature* **473**, 43-49.

Euskirchen, G. M., Auerbach, R. K., Davidov, E., Gianoulis, T. A., Zhong, G., Rozowsky, J., Bhardwaj, N., Gerstein, M. B. and Snyder, M. (2011). Diverse

Development (2015) 142, 1418-1430 doi:10.1242/dev.109496

roles and interactions of the SWI/SNF chromatin remodeling complex revealed using global approaches. *PLoS Genet.* **7**, e1002008.

Gelbart, M. E., Bachman, N., Delrow, J., Boeke, J. D. and Tsukiyama, T. (2005). Genome-wide identification of Isw2 chromatin-remodeling targets by localization of a catalytically inactive mutant. *Genes Dev.* **19**, 942-954.

Gottlieb, P. D., Pierce, S. A., Sims, R. J., Yamagishi, H., Weihe, E. K., Harriss, J. V., Maika, S. D., Kuziel, W. A., King, H. L., Olson, E. N. et al. (2002). Bop encodes a muscle-restricted protein containing MYND and SET domains and is essential for cardiac differentiation and morphogenesis. *Nat. Genet.* **31**, 25-32.

Hang, C. T., Yang, J., Han, P., Cheng, H.-L., Shang, C., Ashley, E., Zhou, B. and Chang, C.-P. (2010). Chromatin regulation by Brg1 underlies heart muscle development and disease. *Nature* **466**, 62-67.

Haraguchi, S., Kitajima, S., Takagi, A., Takeda, H., Inoue, T. and Saga, Y. (2001). Transcriptional regulation of Mesp1 and Mesp2 genes: differential usage of enhancers during development. *Mech. Dev.* **108**, 59-69.

Hnisz, D., Abraham, B. J., Lee, T. I., Lau, A., Saint-André, V., Sigova, A. A., Hoke, H. A. and Young, R. A. (2013). Super-enhancers in the control of cell identity and disease. *Cell* **155**, 934-947.

Ho, L. and Crabtree, G. R. (2010). Chromatin remodelling during development. *Nature* **463**, 474-484.

Ho, L., Ronan, J. L., Wu, J., Staahl, B. T., Chen, L., Kuo, A., Lessard, J., Nesvizhskii, A. I., Ranish, J. and Crabtree, G. R. (2009). An embryonic stem cell chromatin remodeling complex, esBAF, is essential for embryonic stem cell self-renewal and pluripotency. *Proc. Natl. Acad. Sci. USA* **106**, 5181-5186.

Ho, L., Miller, E. L., Ronan, J. L., Ho, W. Q., Jothi, R. and Crabtree, G. R. (2011). esBAF facilitates pluripotency by conditioning the genome for LIF/STAT3 signalling and by regulating polycomb function. *Nat. Cell Biol.* **13**, 903-913.

Hu, G., Schones, D. E., Cui, K., Ybarra, R., Northrup, D., Tang, Q., Gattinoni, L., Restifo, N. P., Huang, S. and Zhao, K. (2011). Regulation of nucleosome landscape and transcription factor targeting at tissue-specific enhancers by BRG1. *Genome Res.* **21**, 1650-1658.

Ishitobi, H., Wakamatsu, A., Liu, F., Azami, T., Hamada, M., Matsumoto, K., Kataoka, H., Kobayashi, M., Choi, K., Nishikawa, S.-i. et al. (2011). Molecular basis for Flk1 expression in hemato-cardiovascular progenitors in the mouse. *Development* **138**, 5357-5368.

Jiang, H., Shukla, A., Wang, X., Chen, W.-Y., Bernstein, B. E. and Roeder, R. G. (2011). Role for Dpy-30 in ES cell-fate specification by regulation of H3K4 methylation within bivalent domains. *Cell* **144**, 513-525.

Kattman, S. J., Witty, A. D., Gagliardi, M., Dubois, N. C., Niapour, M., Hotta, A., Ellis, J. and Keller, G. (2011). Stage-specific optimization of activin/nodal and BMP signaling promotes cardiac differentiation of mouse and human pluripotent stem cell lines. *Cell Stem Cell* **8**, 228-240.

Ku, M., Koche, R. P., Rheinbay, E., Mendenhall, E. M., Endoh, M., Mikkelsen, T. S., Presser, A., Nusbaum, C., Xie, X., Chi, A. S. et al. (2008). Genomewide analysis of PRC1 and PRC2 occupancy identifies two classes of bivalent domains. *PLoS Genet.* **4**, e1000242.

Kwon, H., Imbalzano, A. N., Khavari, P. A., Kingston, R. E. and Green, M. R. (1994). Nucleosome disruption and enhancement of activator binding by a human SW1/SNF complex. *Nature* **370**, 477-481.

Langmead, B., Trapnell, C., Pop, M. and Salzberg, S. L. (2009). Ultrafast and memory-efficient alignment of short DNA sequences to the human genome. *Genome Biol.* **10**, R25.

Lee, T. I., Jenner, R. G., Boyer, L. A., Guenther, M. G., Levine, S. S., Kumar, R. M., Chevalier, B., Johnstone, S. E., Cole, M. F., Isono, K.-i. et al. (2006). Control of developmental regulators by Polycomb in human embryonic stem cells. *Cell* **125**, 301-313.

Marson, A., Levine, S. S., Cole, M. F., Frampton, G. M., Brambrink, T., Johnstone, S., Guenther, M. G., Johnston, W. K., Wernig, M., Newman, J. et al. (2008). Connecting microRNA genes to the core transcriptional regulatory circuitry of embryonic stem cells. *Cell* **134**, 521-533.

Morris, S. A., Baek, S., Sung, M.-H., John, S., Wiench, M., Johnson, T. A., Schiltz, R. L. and Hager, G. L. (2014). Overlapping chromatin-remodeling systems collaborate genome wide at dynamic chromatin transitions. *Nat. Struct. Mol. Biol.* **21**, 73-81.

Narlikar, G. J., Fan, H.-Y. and Kingston, R. E. (2002). Cooperation between complexes that regulate chromatin structure and transcription. *Cell* **108**, 475-487.

Nelson, T. J., Faustino, R. S., Chiriac, A., Crespo-Diaz, R., Behfar, A. and Terzic, A. (2008). CXCR4+/FLK-1+ biomarkers select a cardiopoietic lineage from embryonic stem cells. *Stem Cells* **26**, 1464-1473.

Nix, D. A., Courdy, S. J. and Boucher, K. M. (2008). Empirical methods for controlling false positives and estimating confidence in ChIP-Seq peaks. *BMC Bioinformatics* **9**, 523.

Okano, M., Bell, D. W., Haber, D. A. and Li, E. (1999). DNA methyltransferases Dnmt3a and Dnmt3b are essential for de novo methylation and mammalian development. *Cell* **99**, 247-257.

Parker, S. C. J., Stitzel, M. L., Taylor, D. L., Orozco, J. M., Erdos, M. R., Akiyama, J. A., van Bueren, K. L., Chines, P. S., Narisu, N., Black, B. L. et al. (2013). Chromatin stretch enhancer states drive cell-specific gene regulation and harbor human disease risk variants. *Proc. Natl. Acad. Sci. USA* **110**, 17921-17926.

Rada-Iglesias, A., Bajpai, R., Swigut, T., Brugmann, S. A., Flynn, R. A. and Wysocka, J. (2011). A unique chromatin signature uncovers early developmental enhancers in humans. *Nature* **470**, 279-283.

Reyes, J. C., Barra, J., Muchardt, C., Camus, A., Babinet, C. and Yaniv, M. (1998). Altered control of cellular proliferation in the absence of mammalian brahma (SNF2alpha). *EMBO J.* **17**, 6979-6991.

Sala, A., Toto, M., Pinello, L., Gabriele, A., Di Benedetto, V., Ingrassia, A. M. R., Lo Bosco, G., Di Gesù, V., Giancarlo, R. and Corona, D. F. V. (2011). Genome-wide characterization of chromatin binding and nucleosome spacing activity of the nucleosome remodelling ATPase ISWI. *EMBO J.* **30**, 1766-1777.

Serandour, A. A., Brown, G. D., Cohen, J. D. and Carroll, J. S. (2013). Development of an Illumina-based ChIP-exonuclease method provides insight into FoxA1-DNA binding properties. *Genome Biol.* **14**, R147.

Shi, J., Whyte, W. A., Zepeda-Mendoza, C. J., Milazzo, J. P., Shen, C., Roe, J.-S., Minder, J. L., Mercan, F., Wang, E., Eckersley-Maslin, M. A. et al. (2013). Role of SWI/SNF in acute leukemia maintenance and enhancer-mediated Myc regulation. *Genes Dev.* **27**, 2648-2662.

Stankunas, K., Hang, C. T., Tsun, Z.-Y., Chen, H., Lee, N. V., Wu, J. I., Shang, C., Bayle, J. H., Shou, W., Iruela-Arispe, M. L. et al. (2008). Endocardial Brg1 represses ADAMTS1 to maintain the microenvironment for myocardial morphogenesis. *Dev. Cell* **14**, 298-311.

Surface, L. E., Thornton, S. R. and Boyer, L. A. (2010). Polycomb group proteins set the stage for early lineage commitment. *Cell Stem Cell* **7**, 288-298.

Takeuchi, J. K. and Bruneau, B. G. (2009). Directed transdifferentiation of mouse mesoderm to heart tissue by defined factors. *Nature* **459**, 708-711.

Takeuchi, J. K., Lou, X., Alexander, J. M., Sugizaki, H., Delgado-Olguín, P., Holloway, A. K., Mori, A. D., Wylie, J. N., Munson, C., Zhu, Y. et al. (2011). Chromatin remodelling complex dosage modulates transcription factor function in heart development. *Nat. Commun.* **2**, 187.

Tamkun, J. W., Deuring, R., Scott, M. P., Kissinger, M., Pattatucci, A. M., Kaufman, T. C. and Kennison, J. A. (1992). brahma: a regulator of Drosophila homeotic genes structurally related to the yeast transcriptional activator SNF2/SWI2. *Cell* **68**, 561-572.

Tie, F., Banerjee, R., Conrad, P. A., Scacheri, P. C. and Harte, P. J. (2012). Histone demethylase UTX and chromatin remodeler BRM bind directly to CBP and modulate acetylation of histone H3 lysine 27. *Mol. Cell. Biol.* **32**, 2323-2334.

Wamstad, J. A., Alexander, J. M., Truty, R. M., Shrikumar, A., Li, F., Eilertson, K. E., Ding, H., Wylie, J. N., Pico, A. R., Capra, J. A. et al. (2012). Dynamic and coordinated epigenetic regulation of developmental transitions in the cardiac lineage. *Cell* **151**, 206-220.

Wang, W., Cote, J., Xue, Y., Zhou, S., Khavari, P. A., Biggar, S. R., Muchardt, C., Kalpana, G. V., Goff, S. P., Yaniv, M. et al. (1996). Purification and biochemical heterogeneity of the mammalian SWI-SNF complex. *EMBO J.* **15**, 5370-5382.

Whyte, W. A., Orlando, D. A., Hnisz, D., Abraham, B. J., Lin, C. Y., Kagey, M. H., Rahl, P. B., Lee, T. I. and Young, R. A. (2013). Master transcription factors and mediator establish super-enhancers at key cell identity genes. *Cell* **153**, 307-319.

Wu, J. I., Lessard, J. and Crabtree, G. R. (2009). Understanding the words of chromatin regulation. *Cell* **136**, 200-206.

Yu, Y., Chen, Y., Kim, B., Wang, H., Zhao, C., He, X., Liu, L., Liu, W., Wu, L. M. N., Mao, M. et al. (2013). Olig2 targets chromatin remodelers to enhancers to initiate oligodendrocyte differentiation. *Cell* **152**, 248-261.

Yuan, W., Wu, T., Fu, H., Dai, C., Wu, H., Liu, N., Li, X., Xu, M., Zhang, Z., Niu, T. et al. (2012). Dense chromatin activates Polycomb repressive complex 2 to regulate H3 lysine 27 methylation. *Science* **337**, 971-975.

Zhang, C. L., McKinsey, T. A., Chang, S., Antos, C. L., Hill, J. A. and Olson, E. N. (2002). Class II histone deacetylases act as signal-responsive repressors of cardiac hypertrophy. *Cell* **110**, 479-488.

Zhou, V. W., Goren, A. and Bernstein, B. E. (2011). Charting histone modifications and the functional organization of mammalian genomes. *Nat. Rev. Genet.* **12**, 7-18.

Supplementary Material

I Supplemental Methods

Cardiomyocyte differentiation

Mouse ES cells were aggregated into embryoid bodies (EB) and cultured at 75,000 cells/ml for two days in serum free media (3 parts IMDM (Cellgro #15-016-CV): 1 part Ham's F12 (Cellgro #10-080-CV), 0.05% BSA, 2 mM GlutaMax (Gibco), B27 supplement (Gibco #12587010), N2 supplement (Gibco #17502048)) supplemented with 50 ug/ml ascorbic acid and 4.5 x 10^{-4} M monothioglycerol. Embryoid bodies were dissociated and reaggregated for 40 hours in the presence of 5 ng/mL human VEGF (R&D #293-VE) and human Activin A (R&D #338-AC) and human BMP4 (R&D #314-BP) at concentrations empirically determined depending on lot. EBs were dissociated and plated at 470,000 cells/cm^2 in StemPro-34 (Gibco #10639011) supplemented with 2 mM GlutaMax, 50 ug/mL ascorbic acid, 5 ng/mL VEGF, 10 ng/mL human basic FGF (R&D #233-FB) and 25 ng/mL FGF10 (R&D #345-FG) for two days. After two days, StemPro-34 with GlutaMax and ascorbic acid was used and replaced daily.

For Brg1 deletion studies, *Brg1*$^{fl/fl}$;*Actin-CreER* ES cells (Ho et al., 2009, Ho et al., 2011) were cultured and differentiated as described above. Cultures were treated with 200 nM 4-hydroxytamoxifen (4-OHT) diluted from a 5 mg/mL stock solution in tetrahydrofuran (THF) or with only THF for control. Fresh 4-OHT was added with each media change. For cell viability studies, dead cells were identified using Trypan blue.

Flow cytometry

For cell surface staining, cells were briefly trypsinized, quenched with serum, and

washed in FACS Buffer (4% FBS in D-PBS) four times. After washing, cells were stained with a biotinylated anti-FLK-1 (Hybridoma Clone D218) antibody for 30 minutes at 4°C. Cells were then washed three times in FACS Buffer and stained with a PE-conjugated anti-PDGFRα (eBioscience 12-1401-81, 1:400) and APC-Streptavidin (1:200) for 30 minutes at 4°C. Cells were three times in FACS Buffer and analyzed on an LSRII flow cytometer (BD). Data was analyzed using FlowJo software (Treestar).

For intracellular staining, cultures were trypsinized, quenched with serum, and fixed in D-PBS with 3.7% formaldehyde for 30 minutes at room temperature. Fixed samples were washed twice and stained with anti-cTnT (Thermo Scientific #MS295, Clone 13-11). antibody. After staining, samples were washed twice, incubated with secondary antibody, and washed two additional times. All steps performed in D-PBS with 0.5% saponin and 4% FBS. Samples were stained with Hoechst 33342 (10 ug/mL) in D-PBS with 4% FBS. Samples were analyzed as above.

Quantitative PCR

RNA was extracted using TRIzol® and reversed transcribed using High-Capacity cDNA Reverse Transcription kit (Applied). Quantitative PCR was performed in technical triplicate using Taqman probes and expression was normalized to *Gapdh*. The following probes were used: *Mesp1* – Mm00801883_g1, *Gapdh* – 4352932E

Western blotting

Western blotting was performed using standard techniques. Briefly, protein lysate was sonicated (4 pulses for 30 seconds) and cleared by centrifugation at 13,000 RPM. Supernatant was diluted 1:1 with 2x Laemmli Buffer and 100 mM DTT and boiled for 10 minutes at 95°C. Following electrophoresis, protein was transferred to a PVDF

membrane. Membranes were blocked for 1 hour at room temperature with 5% milk Tris-buffered saline Tween (TBST). Following blocking, membranes were incubated with desired antibody in 5% milk TBST overnight at 4°C. Membranes were washed 4 times for 15 minutes at room temperature in TBST and then stained with secondary antibody in 5% milk TBST for 1 hour at room temperature. After antibody staining, membranes were washed as after primary incubation, incubated in SuperSignal chemiluminescence substrate (Thermo Scientific), and visualized. Antibodies used were anti-BRG1 (Santa Cruz sc-10768), anti-actin (Sigma A1978), and anti-FLAG (Sigma M2).

Immunofluorescence

Cultures were fixed for 30 minutes at room temperature in 3.7% formaldehyde D-PBS and washed once with D-PBS. Wells were blocked in 2% bovine serum albumin 0.1% Triton-X-100 D-PBS for 30 minutes at RT. After blocking, cultures were incubated with primary antibody at 4°C overnight. Slides were washed three times with 0.1% Triton X-100 D-PBS and incubated in secondary antibody at room temperature for 1 hour. After staining, slides were washed three times with 0.1% Triton X-100 D-PBS, stained with Hoechst 33342 (10 ug/mL) in D-PBS, and immediately imaged in 50 uL D-PBS. Antibodies used were anti-cardiac isoform of Troponin T (cTnT) 1:100 (Thermo Scientific #MS295, Clone 13-11).

Transfections

HeLa cells were transfected with 1 ug of plasmid using X-tremeGene (Roche) and cells were harvested 42 hrs after transfection.

ChIP-Seq / ChIP-exo

Frozen pellets of cross-linked cells ($10x10^6$) were thawed in cold lysis buffer 1 (50 mM HEPES-KOH, pH 7.5, 140 mM NaCl, 1 mM EDTA, 10% glycerol, 0.5% NP-40, 0.25% Triton X-100, 1× protease inhibitors) and gently rocked at 4°C for 10 minutes in 15 mL conical tubes. Cells were pelleted at 1350 x g at 4°C and resuspended in cold lysis buffer 2 (10 mM Tris-HCl, pH 8.0, 200 mM NaCl, 1 mM EDTA, 0.5 mM EGTA, 1× protease inhibitors) and gently rocked at 4°C for 10 minutes in 15 mL conical tubes. Cells were pelleted at 1350 x g at 4°C in a table top centrifuge and resuspended in 0.5 mL cold ChIP lysis buffer (50 mM HEPES-NaOH, pH 7.5, 140 mM NaCl, 1 mM EDTA, 1% Triton X-100, 0.1% SDS, 0.1% sodium deoxycholate) and sonicated to 200-1000 bp fragments using a VirSonic sonicator. Sonicated lysates were cleared by pelleting insoluble material at 13,000 RPM at 4°C followed by incubation with 5 ug antibody overnight. Next, Protein A magnetic beads (45 uL) were added to the lysate and incubated at 4°C for 7 hrs. Prior to addition, magnetic beads were washed 3 times with block (0.5% BSA/PBS). Immunoprecipitated material was washed 2 times each with ChIP lysis buffer, high salt lysis buffer (50 mM HEPES-NaOH pH 7.5, 500 mM NaCl, 1 mM EDTA, 1% Triton X-100, 0.1% SDS, 0.1% sodium deoxycholate), and LiCl wash buffer (10 mM Tris-HCl pH 8.0, 250 mM LiCl, 1 mM EDTA, 0.5% NP-40, 0.5% sodium deoxycholate) and one time with TE plus NaCl, followed by elution and reverse crosslinking in 210 uL of 1% SDS in TE overnight at 65°C. 200 uL of uncrosslinked material was treated with RNase A for 2 hours, proteinase K for 2 hours, and extracted 2 times with phenol/chloroform/isoamyl alcohol. This was followed by ethanol precipitation with a glycogen coprecipitant, 80% ethanol wash and final resuspension in TE. Nucleic acid yield was determined via PicoGreen (Invitrogen). Adapter ligation and size selection (200-400 bp) were performed using a Beckman Coulter SPRI TE nucleic acid extractor,

or, in some cases, performed by hand. Fragments were PCR amplified for 13 cycles followed by sequencing on an Illumina HiSeq 2000 system. For hand prepared libraries, libraries were made using the Ovation Library Prep kit according the manufacturer's instructions (NuGen). Briefly, DNA samples were end repaired, ligated to adaptors, and purified using AMPure beads. Purified samples were amplified by PCR for 17 cycles, purified, and sequenced on an Illumina HiSeq 2000 system.

For BRG1-FLAG ChIP-seq, the protocol described above was followed except 8-10x10^6 cells were used as starting material and 10 ug antibody was incubated with Protein G magnetic beads for roughly 6 hours prior to washing and addition of the bead/antibody complex to chromatin lysate for immunoprecipitation overnight.

Brg1 ChIP-exo was performed as previously described (Serandour et al., 2013) using anti-BRG1 antibody (1mg, Abcam 110641). ChIPExo was performed on Brg1 ChIP material while still on protein G magnetic dynabeads. After incubation with the antibody, the beads were washed six times with RIPA buffer (50mM HEPES, pH7.6, 1mM EDTA, pH8.0, 0.7% Sodium deoxycholate, 1% NP-40 and 500mM Lithium chloride) and two times with Tris (10mM Tris.Cl, pH 8.0). The bead bound DNA were end polished at 30°C for 30mins in using T4 DNA polymerase, Klenow fragment of DNA polymerase and T4 polynucleotide kinase. From this point each subsequent enzymatic steps were followed by two washes with each of RIPA and 10mM Tris. P7 adapter was ligated to the DNA ends using T4 DNA ligase at 25°C for 60 mins followed by nick repair using Phi29 polymerase at 30°C for 20 mins. Samples were periodically vortexed at 900rpm in a thermomixure during enzymatic reaction. DNA was digested with λ and RecJf exonucleases at 37°C for 30 mins each. Samples were then eluted off the beads with 100μl of Elution buffer (50mM Tris.Cl, pH 8.0, 10mM EDTA, 1% SDS) by incubating at

65°C for 30mins with periodic shaking. RNase A was added to the samples for 30min at 37°C. Proteinase K was added to degrade proteins, crosslink was reversed by overnight incubation at 65°C and using Ampure beads ChIP DNA was purified. The purified DNA was denatured at 95°C for 5 mins before synthesis of the 2nd strand by P7 primer extension in presence of Phi29 polymerase. Then, P5 adapters were ligated to the DNA ends and the DNA fragments were PCR amplified for 18 cycles using universal primers containing the index sequences. PCR products were purified using Ampure beads, size selected using 2% agarose gels in an E-Gel Electrophoresis system (Invitrogen), gel purified using minielute gel extraction columns (Qiagen) and eluted in 20μl of TE. Samples were quantified and analysed on Qubit and Bioanalyser before sequencing on a Illumina HiSeq 2500 sequencing machine.

ChIP-seq/ChIP-exo analysis pipeline

Single end 40 bp reads were aligned to the mouse genome (mm9) using Bowtie (Langmead et al., 2009). Unique sequences were extended +200 bp and allocated in 25-bp bins. Input DNA was used as a background model. A Poissonian model was used to determine statistically enriched bins with a P-value threshold set at 1x10^{-12} for H3K27me3, H3K27ac, and Suz12 and 1x10^{-6} for Flag-Brg1 as described previously (Marson et al., 2008). Genomic browser tracks were generated using the Integrated Genome Viewer (Robinson et al., 2011). Browser tracks and other downstream analysis was performed on pooled data from multiple replicates. Similar trends were observed if replicates were analyzed individually.

Computational analysis

Chromatin regulator expression

To visualize expression patterns for annotated chromatin regulators, chromatin regulators annotated as involved in chromatin remodeling (GO0006338) or covalent chromatin modification (GO00016569) were considered. Genes *Smarca2*, *Pbrm1*, *Arid1b*, *Smarcd3*, *Smarcd2*, *Phf10*, *Dpf1*, *Dpf2*, *Dpf3*, *Smarce1*, *Arid2*, and *Arid1a* were manually added to this list based on the literature. The median expression values of these genes for four stages of cardiac differentiation (Wamstad et al., 2012) were median centered and interquartile range scaled and clustered using the bioconductor package Hopach (http://www.bioconductor.org/packages/2.1/bioc/html/hopach.html) and a cosine angle distance metric.

Tissue and cell type expression of upregulated developmental TFs

Normalized expression data from the Gene Atlas GNF1M dataset (Su et al., 2004) for upregulated developmental TFs were averaged (mean) between replicates and visualized as a heatmap. Developmental TFs were identified as genes that are annotated as within both GO terms GO0003700 (sequence-specific DNA binding transcription factor activity) and GO0048856 (anatomical structure development).

Classification of BRG1 peaks, enhancers, and H3K27me3 domains

To identify BRG1 bound regions, we overlapped statistically enriched peaks over two replicates of FLAG ChIP-seq and required peaks in both replicates to be within 1 kb. Calling peak overlap within 500 bp reduces the number of called peaks by less than 10%, and not much more by calls within 250 bp, indicating that concordant peaks overlap well. Peaks conserved across replicates were then merged into a single region that included both peaks and any genomic space in between. In order to classify genomic localization of BRG1 bound regions, Ensembl lists of genes and exons were

intersected with BRG1 enriched regions. Promoter regions were classified as ±2.5 kb of the TSS. If a BRG1 bound region overlapped with more than one classification, it was labeled according to the following order: Promoter > Exon > Intron > Intergenic. Thus all peaks that did not overlap with promoters, exons, or introns were labeled intergenic. Putative enhancer regions were identified by intersecting regions of H3K27ac enrichment for both biological replicates. The size of the enhancer represents the combined length of the enriched regions for each replicate. Blocks of genomic space ± 2.5 kb from the Ensembl TSSs were subtracted to yield a list of high-confidence putative distal enhancers. To determine the proportion of Brg1 peaks that fall within putative enhancers, we intersected these regions, requiring at least one base pair of overlap.

To identify enhancers associated with blocks labeled “super” enhancers, we utilized the ROSE (https:// bitbucket.org/young_computation/rose) algorithm that has been previously described (Hnisz et al., 2013). Briefly, enhancers within 12.5 kb were merged and ranked according to input-subtracted signal of H3K27ac, which is used to determine a H3K27ac signal inflection point and identify super enhancers. Enhancers within ± 2.5 kb of the TSS were excluded from this analysis. These domains of “super” enhancers were then intersected with all identified enhancers to identify enhancers associated with super enhancer domains.

Motif enrichment within BRG1+ enhancers was done by scanning the subset of BRG1-bound regions that completely overlapped with a putative enhancer using TRANSFAC's 'match' algorithm for whether or not each vertebrate motif in the database was identified within 75 bp of the center of that enriched region, and the hypergeometric distribution was used to calculate the probability that a given number of each motif would be seen among BRG1-associated peaks, given its abundance among all H3K27-acetylated

enhancers, and the false discovery rates for these probabilities were controlled using the q-value (Storey and Tibshirani, 2003). Each enriched motif was annotated with the expression at each stage of in vitro cardiomyocyte differentiation using data from (Wamstad et al., 2012).

Replicate Correlation

Unique sequence were extended by 200 bp and allocated into 20 bp bins. Bin read density was calculated and compared across all genomic bins using a Spearman's rank correlation.

Visualization of ChIP-seq data

To determine the average profile of H3K27me3, H3K27ac, or SUZ12 ChIP-seq and Input signal around transcriptional start sites or enhancer regions, unique aligned reads within 5 kb of the TSS or the midpoint of enhancer regions were grouped into 50 bp bins and then normalized based on number of reads per library (reads per million). In cases where the ChIP-seq read density of many promoters or regions of interest were visualized together, normalized binned read counts for each gene were visualized as heatmaps using R. For boxplots, a normalized read count was computed ±5 kb from the TSS. For boxplots for enhancer regions, a $\log_2$ fold change in normalized read count was computed between conditions for each predicted enhancer region or subset of enhancers investigated.

Polycomb target analysis

TSSs were extended 1 kb in each direction and compared to genome-wide data sets for H3K27me3 and Polycomb subunits in ES cells (Ku et al., 2008) to identify overlap.

Transcriptional start sites for all Refseq genes and genes corresponding to these significantly upregulated or downregulated based on the RNA-seq analysis were considered. A hypergeometric test was used to determine statistical significance and calculate p-values for this comparison.

Statistical Analysis

To look for statistical enrichment of BRG1 and enhancer overlap, we generated 10,000 lists of randomly generated enhancer regions of identical size to our experimentally-derived list. We then intersected each random list with BRG1 bound regions to generate a normal distribution of expected overlap. P-value represents the number of permutations over our random enhancer lists with equal or more overlap than our experimental list.

II. Supplementary Datasets

Supplemental Table 1.

Median centered and interquartile range scaled RPKM expression values for chromatin regulators during directed cardiomyocyte differentiation of embryonic stem cells (Wamstad et al. 2012). Chromatin regulators are genes found in GO categories GO0006338 and GO00016569 and other manually curated genes.

Supplemental Table 2.

Differential gene expression between Day4 4OHT and Day4 Control treated Brg1f/f; Actin-CreER ESCs. Gene list is filtered to remove any genes not expressed above 0.5 RPKM in either condition. Includes genes significantly downregulated or upregulated at a false discovery rate of 1% and three fold change cutoffs (1.2x, 1.5x, and 2.0x).

Supplemental Table 3.

Enriched Gene Ontology terms for significantly downregulated and upregulated genes. Tables are standard output for GOElite.

Supplemental Table 4.

Putative enhancer list: Predicted enhancer regions in mesodermal cultures based on H3K27ac enrichment. Table includes genomic coordinates for each putative enhancer region and the gene with the closest transcriptional start site.

Brg1 enriched regions: Table with the genomic coordinates of BRG1 enriched regions in mesodermal cultures. Brg1 Enriched Regions are the combined length of Brg1 peaks within 1 kb of each other in both replicates from BRG1-FLAG mESCs, including genomic sequence between the peaks.

III. Supplemental Figure Legends

Fig S1. Loss of *Brg1* during mesoderm differentiation reduces viable cells in cardiogenic conditions. (A) Phase contrast images of *Brg1* f/f; Actin-CreER ESCs at Day 11 of directed differentiation demonstrates reduced cell density in cultures treated with 4-OHT at Day 2. Scale bar is 50 μm. (B) Number of viable cells in cultures treated with control or 4-OHT at Day 2 after replating at 150,000 cells per well. Solid and dashed lines indicate two separate differentiations. (C) Treatment of the control ESC line E14 Tg(Nkx2-5-EmGFP) that lacks the Actin-CreER transgene differentiates with comparable efficiency across a range of BMP4 when treated with vehicle control or 200 nM 4-OHT beginning at Day 2 of differentiation. cTnT % was determined by intracellular FACS at Day 10. Three independent differentiations are shown.

Fig S2. Developmental transcription factors upregulated by loss of *Brg1* in mesoderm function in diverse development lineages. Expression levels of 72 developmental transcription factors that are upregulated by loss of *Brg1* in various mouse tissues and cell types. Samples are grouped based on similarities in embryonic origin or function.

Fig S3. Genes upregulated by loss of *Brg1* in mesoderm are lowly expressed in normal mesoderm cultures. Upregulated genes were binned based on their expression decile in normal mesoderm cultures (Day 4 control RNA-seq).

Fig S4. Characterization of *Brg1*-Flag embryonic stem cells. (A) Western blot of protein lysate from *Brg1*-Flag ESC demonstrates robust expression of BRG1-Flag protein. HeLa cells transfected with Flag- and myc- tagged expression constructs serve as positive and negative controls, respectively. (B) Immunoprecipitation of BRG1-Flag from *Brg1*-Flag ESC protein lysate using an anti-Flag antibody and visualized by silver stain. BRG1-Flag co-immunoprecipitates with multiple proteins with molecular weights consistent with known BAF complex components. An immunoprecipitation in the NkxGFP ESC line, which does not express BRG1-Flag, does not pull down these proteins.

Fig S5. Examples of histone modification changes found at misregulated genes in Brg1-deficient mesoderm cultures. (A,B) Tracks for RNA-seq and H3K27ac, H3K27me3, SUZ12, Flag, and Brg1 ChIP-seq/ChIP-exo are shown for genomic regions flanking dysregulated genes. (A) BRG1 binding at putative enhancers proximal to downregulated genes. BRG1 bound enhancers show reduced H3K27ac. (B) Example derepressed genes that demonstrate reduced levels of H3K27me3. Control samples are colored blue and 4-OHT samples are colored red. Tan boxes indicate regions of BRG1 enrichment.

Fig S6. *Brg1* does not affect global levels of H3K27ac at promoters. (**A**) Histogram of $\log_2$ fold change in H3K27ac at Refgene promoters. (**B**) Boxplots of $\log_2$ fold change of subsets of Refgene promoter. N indicates the number of promoters include in each set. (**C**) Boxplots of $\log_2$ fold change of subsets of predicted enhancers. Enhancers are separated into Brg1 bound and unbound cohorts based on the presence or absence of a Brg1 peak respectively. These groups were subdivided into static enhancers (enhancers found in both embryonic stem cells and mesodermal cultures), activated enhancers (enhancers found only in mesodermal cultures), and "super enhancers" (predicted using methods described in (Hnisz et al., 2013)). BRG1 bound, activated enhancers show the greatest average loss in H3K27ac. "Super" enhancers bound by BRG1 had a more modest reduction in H3K27ac than BRG1-bound activated enhancers. N indicates the number of enhancers included in each set. Enhancers and promoters that gave undefined fold change values were excluded. All comparisons significant at $P<0.00001$ (by two-sided KS test).

Fig S7. RPKM values of Polycomb subunits or other H3K27-modifying enzymes in control or 4-OHT treated mesoderm cultures. Loss of *Brg1* does not affect RNA expression of these genes.

Fig S8. Upregulated genes are repressed by Polycomb repressive complexes in embryonic stem cells. Percent of all genes or those upregulated by loss of Brg1 in mesoderm that are marked by H3K27me3 or bound by SUZ12 in ES cells (Ku et al. 2008). Upregulated genes demonstrate significant enrichment for both groups. * $p = 9.03\times10^{-80}$; ** $p=5.15\times10^{-82}$

Supplementary Methods References

Hnisz, D., Abraham, B. J., Lee, T. I., Lau, A., Saint-Andre, V., Sigova, A. A., Hoke, H. A. and Young, R. A. (2013). Super-Enhancers in the Control of Cell Identity and Disease. *Cell*.

Ku, M., Koche, R. P., Rheinbay, E., Mendenhall, E. M., Endoh, M., Mikkelsen, T. S., Presser, A., Nusbaum, C., Xie, X., Chi, A. S., et al. (2008). Genomewide analysis of PRC1 and PRC2 occupancy identifies two classes of bivalent domains. *PLoS Genet* **4**, e1000242.

Langmead, B., Trapnell, C., Pop, M. and Salzberg, S. L. (2009). Ultrafast and memory-efficient alignment of short DNA sequences to the human genome. *Genome Biol* **10**, R25.

Marson, A., Levine, S. S., Cole, M. F., Frampton, G. M., Brambrink, T., Johnstone, S., Guenther, M. G., Johnston, W. K., Wernig, M., Newman, J., et al. (2008). Connecting microRNA genes to the core transcriptional regulatory circuitry of embryonic stem cells. *Cell* **134**, 521-533.

Robinson, J. T., Thorvaldsdottir, H., Winckler, W., Guttman, M., Lander, E. S., Getz, G. and Mesirov, J. P. (2011). Integrative genomics viewer. *Nat Biotechnol* **29**, 24-26.

Serandour, A. A., Brown, G. D., Cohen, J. D. and Carroll, J. S. (2013). Development of an Illumina-based ChIP-exonuclease method provides insight into FoxA1-DNA binding properties. *Genome Biol* **14**, R147.

Storey, J. D. and Tibshirani, R. (2003). Statistical significance for genomewide studies. *Proc Natl Acad Sci U S A* **100**, 9440-9445.

Su, A. I., Wiltshire, T., Batalov, S., Lapp, H., Ching, K. A., Block, D., Zhang, J., Soden, R., Hayakawa, M., Kreiman, G., et al. (2004). A gene atlas of the mouse and human protein-encoding transcriptomes. *Proc Natl Acad Sci U S A* **101**, 6062-6067.

Wamstad, J. A., Alexander, J. M., Truty, R. M., Shrikumar, A., Li, F., Eilertson, K. E., Ding, H., Wylie, J. N., Pico, A. R., Capra, J. A., et al. (2012). Dynamic and coordinated epigenetic regulation of developmental transitions in the cardiac lineage. *Cell* **151**, 206-220.

Supplemental Figures

Fig S1

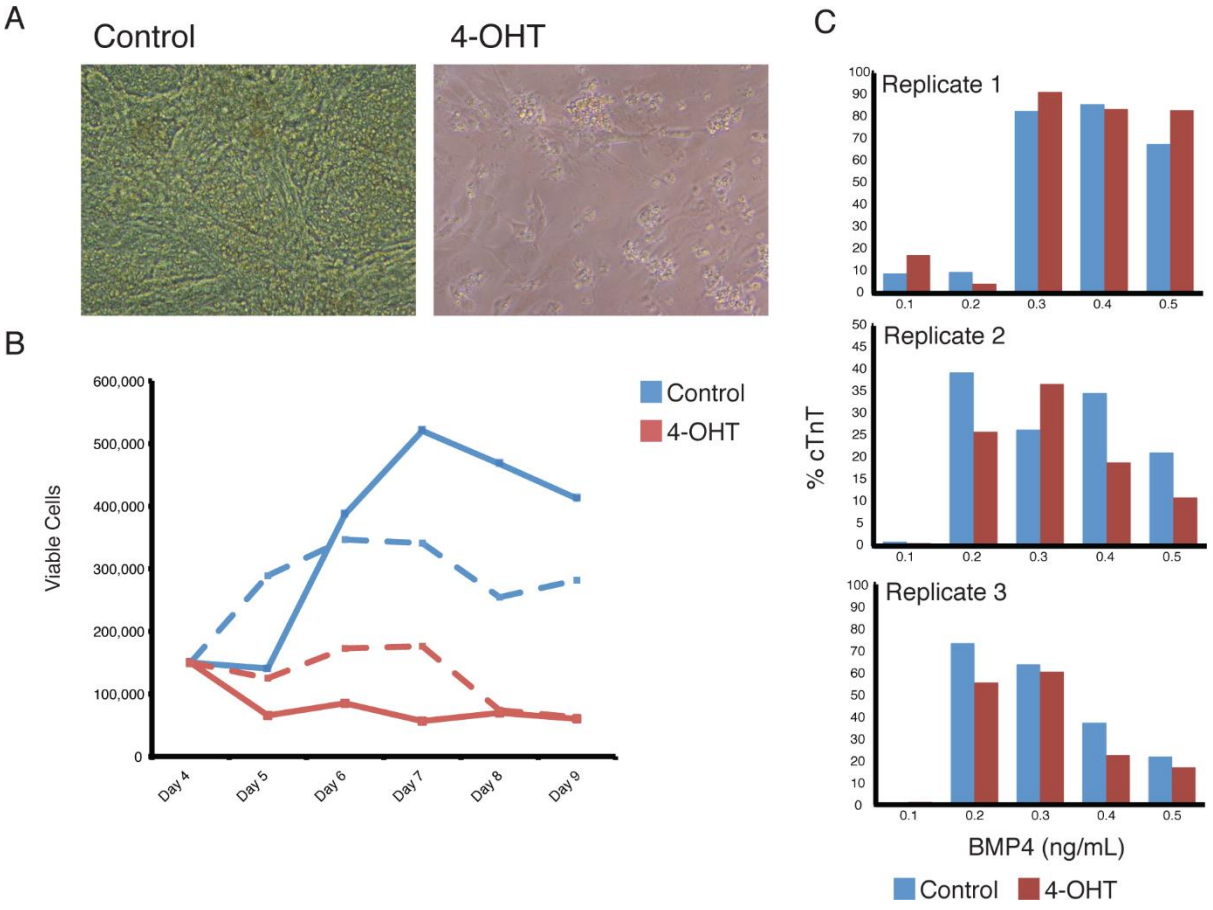

Fig S2

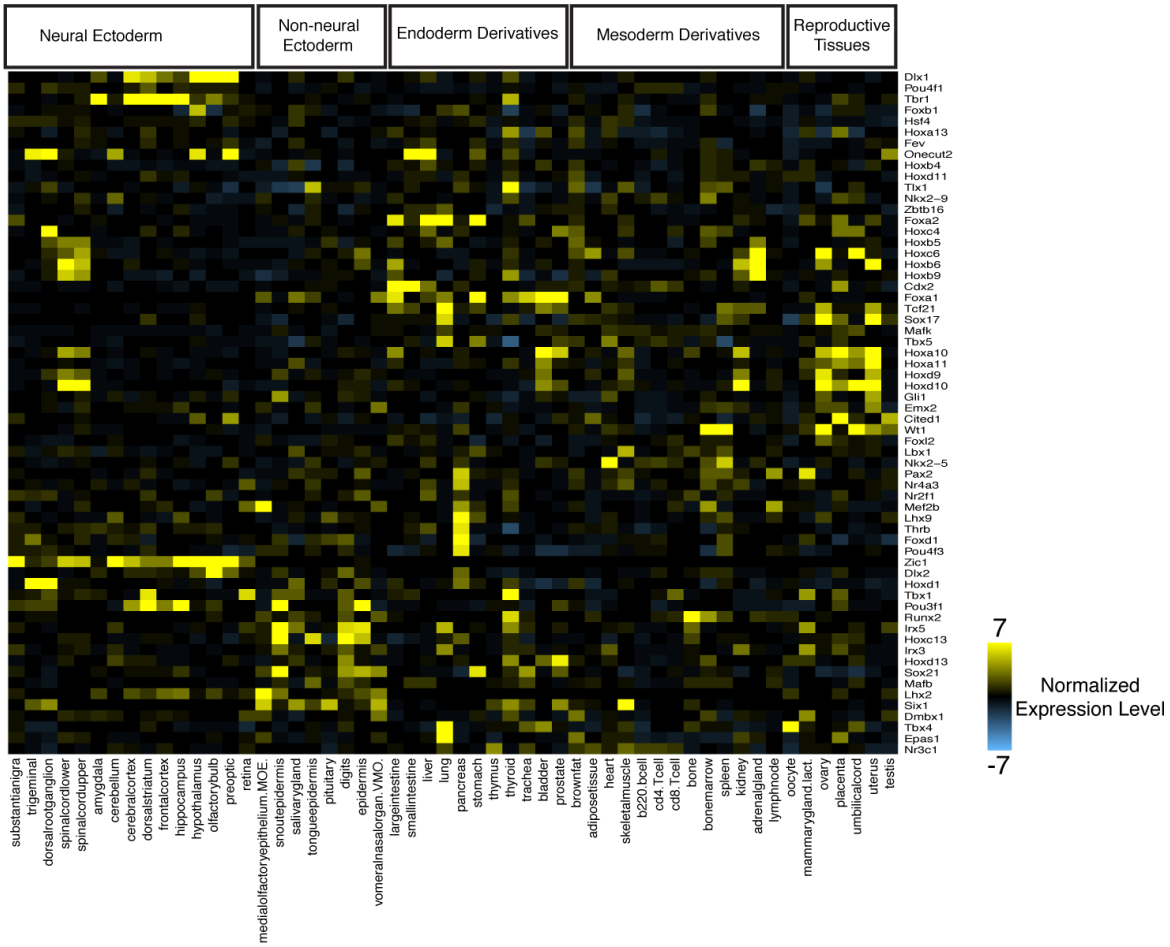
Neural Ectoderm
Non-neural Ectoderm
Endoderm Derivatives
Mesoderm Derivatives
Reproductive Tissues
Dlx1
Pou4f1
Tbr1
Foxb1
Hsf4
Hoxa13
Fev
Onecut2
Hoxb4
Hoxd11
Tlx1
Nkx2-9
Zbtb16
Foxa2
Hoxc4
Hoxb5
Hoxc6
Hoxb6
Hoxb9
Cdx2
Foxa1
Tcf21
Sox17
Mafk
Tbx5
Hoxa10
Hoxa11
Hoxd9
Hoxd10
Gli1
Emx2
Cited1
Wt1
Foxl2
Lbx1
Nkx2-5
Pax2
Nr4a3
Nr2f1
Mef2b
Lhx9
Thrb
Foxd1
Pou4f3
Zic1
Dlx2
Hoxd1
Tbx1
Pou3f1
Runx2
Irx5
Hoxc13
Irx3
Hoxd13
Sox21
Mafb
Lhx2
Six1
Dmbx1
Tbx4
Epas1
Nr3c1
substantianigra
trigeminal
dorsalrootganglion
spinalcordlower
spinalcordupper
amygdala
cerebellum
cerebralcortex
dorsalstriatum
frontalcortex
hippocampus
hypothalamus
olfactorybulb
preoptic
retina
medialolfactoryepithelium.MOE
snoutepidermis
salivarygland
tongueepidermis
pituitary
digits
epidermis
vomeralnasalorgan.VMO.
largeintestine
smallintestine
liver
lung
pancreas
stomach
thymus
thyroid
trachea
bladder
prostate
brownfat
adiposetissue
heart
skeletalmuscle
b220.bcell
cd4.Tcell
cd8.Tcell
bone
bonemarrow
spleen
kidney
adrenalgland
lymphnode
oocyte
mammarygland.lact.
ovary
placenta
umbilicalcord
uterus
testis
7
Normalized Expression Level
-7

Fig S3

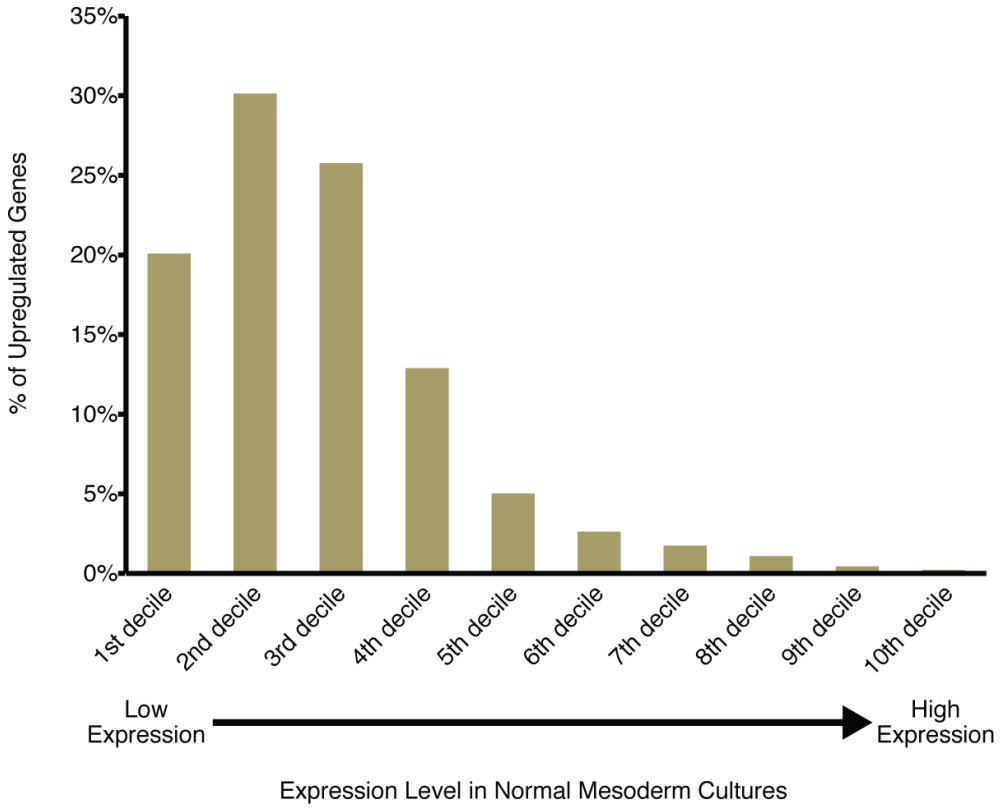
35%
30%
25%
20%
15%
10%
5%
0%
% of Upregulated Genes
1st decile
2nd decile
3rd decile
4th decile
5th decile
6th decile
7th decile
8th decile
9th decile
10th decile
Low Expression
High Expression
Expression Level in Normal Mesoderm Cultures

Fig S4

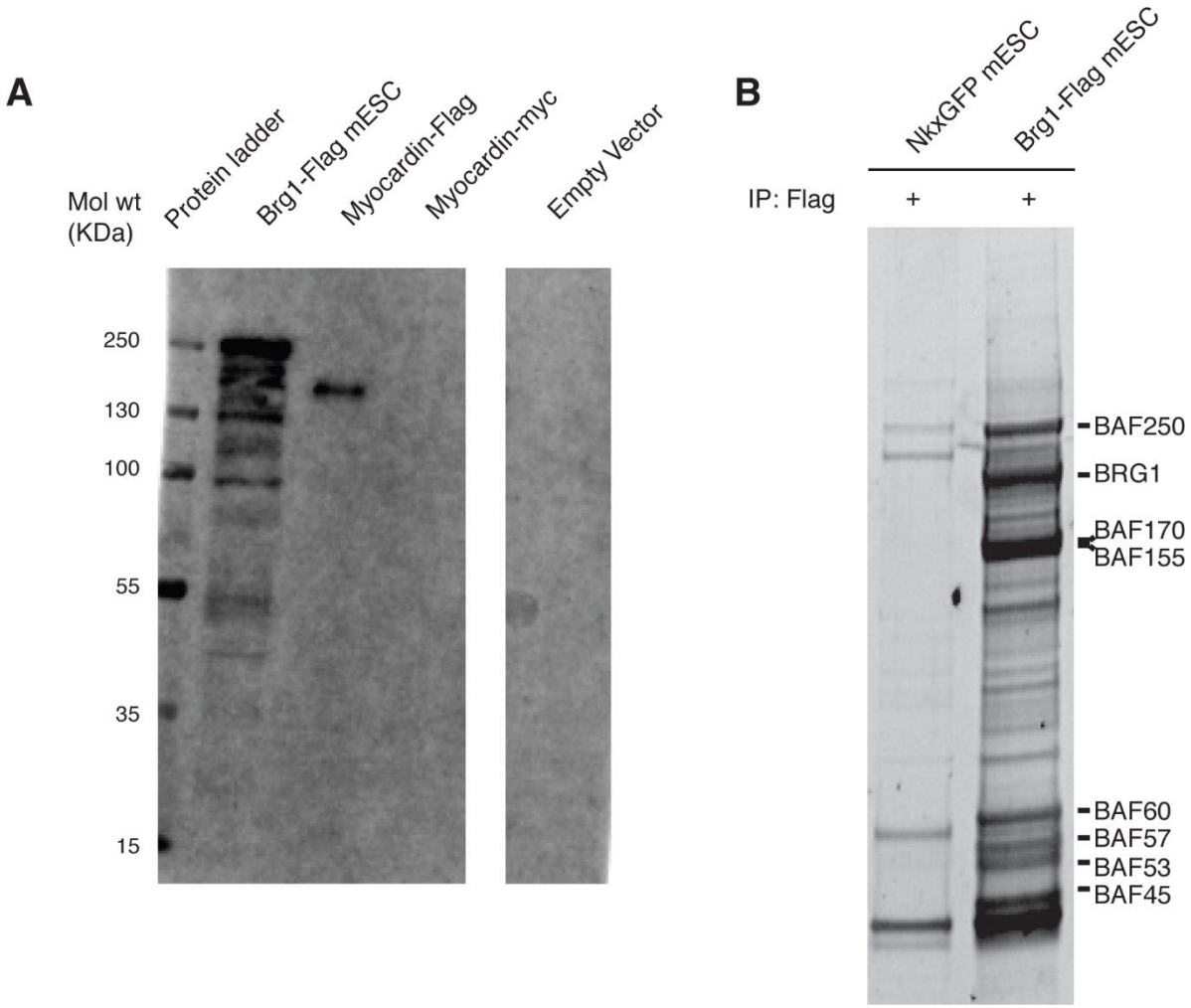
A
Mol wt (KDa)
Protein ladder
Brg1-Flag mESC
Myocardin-Flag
Myocardin-myc
Empty Vector
250
130
100
55
35
15
B
NkxGFP mESC
Brg1-Flag mESC
IP: Flag
+
+
BAF250
BRG1
BAF170
BAF155
BAF60
BAF57
BAF53
BAF45

Fig S5

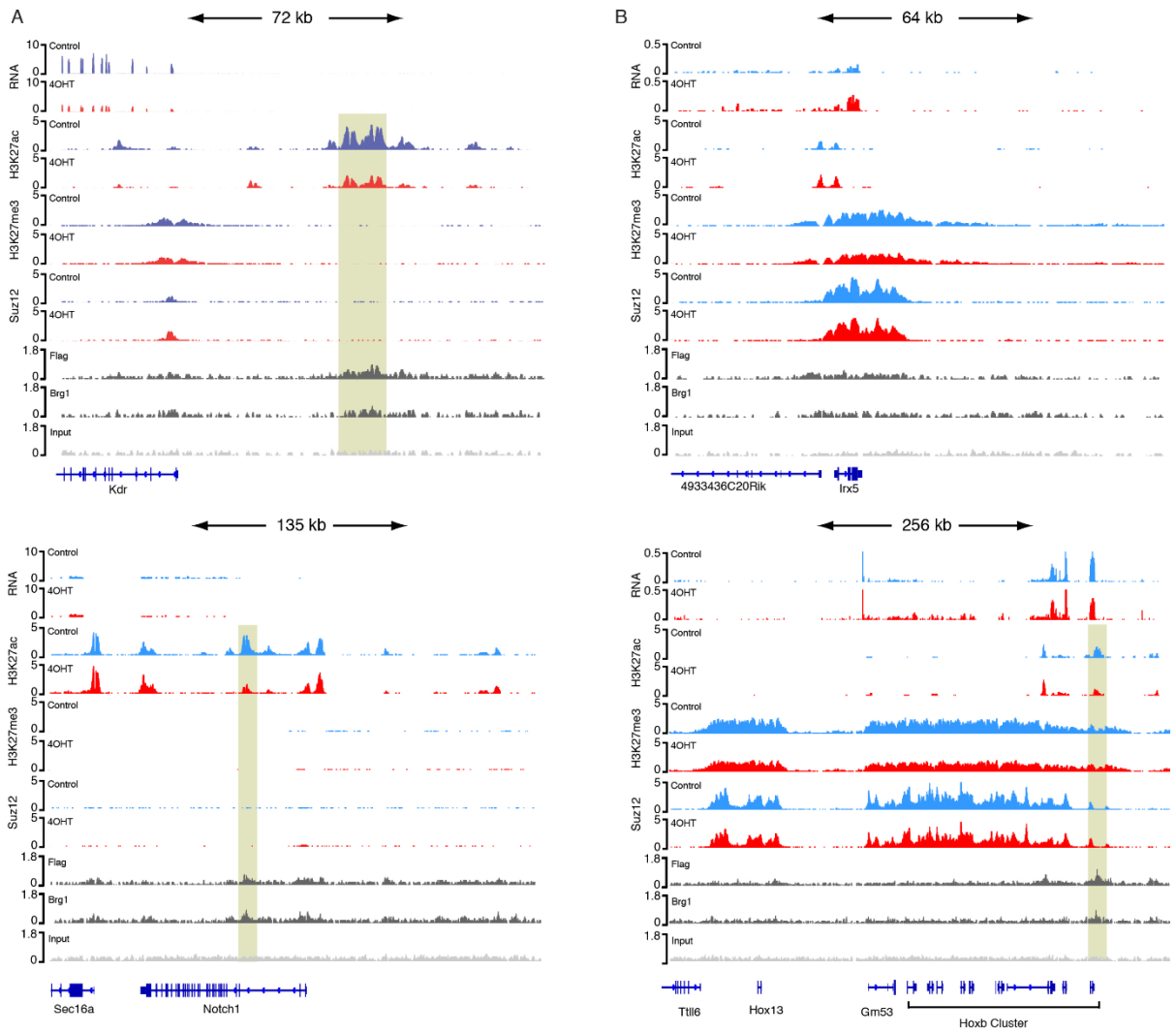
A
72 kb
RNA
H3K27ac
H3K27me3
Suz12
Control
4OHT
Flag
Brg1
Input
Kdr
B
64 kb
4933436C20Rik
Irx5
135 kb
Sec16a
Notch1
256 kb
Ttll6
Hox13
Gm53
Hoxb Cluster

Fig S6

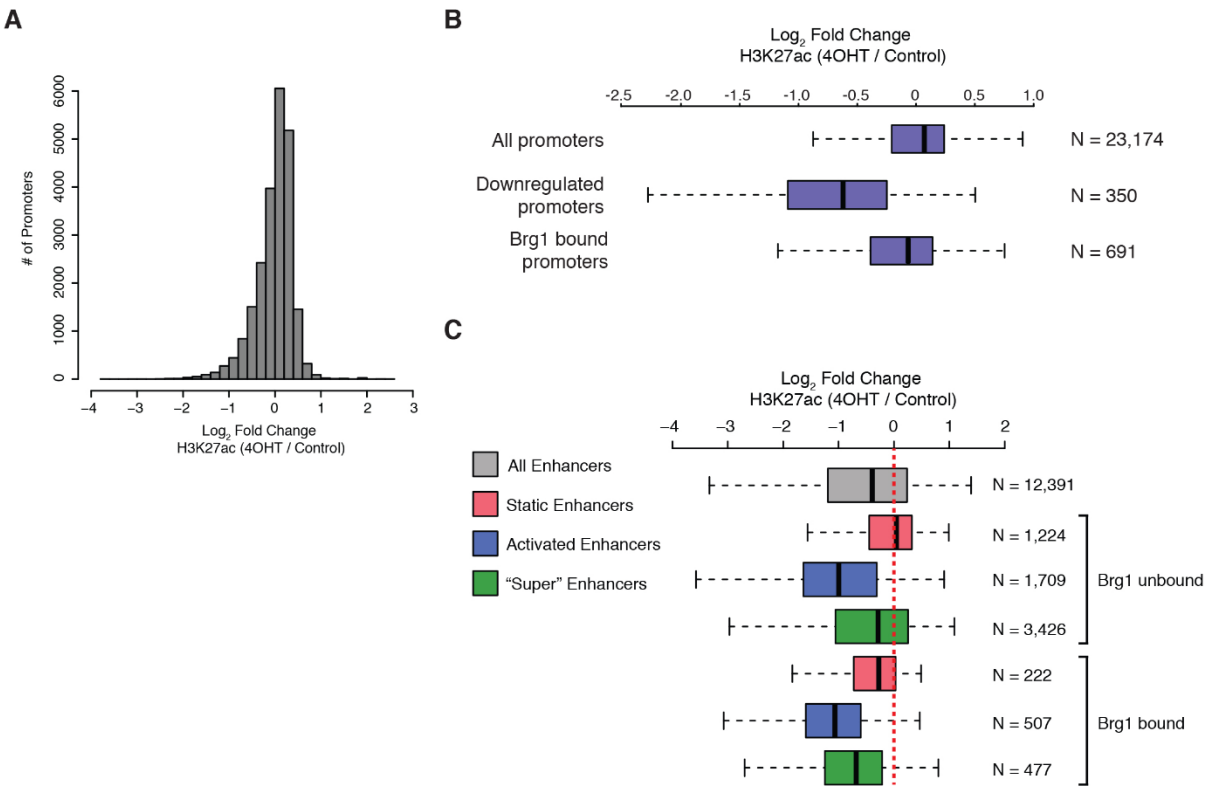
A
# of Promoters
0
1000
2000
3000
4000
5000
6000
−4
−3
−2
−1
0
1
2
3
Log2 Fold Change
H3K27ac (4OHT / Control)
B
Log2 Fold Change
H3K27ac (4OHT / Control)
-2.5
-2.0
-1.5
-1.0
-0.5
0
0.5
1.0
All promoters
N = 23,174
Downregulated promoters
N = 350
Brg1 bound promoters
N = 691
C
Log2 Fold Change
H3K27ac (4OHT / Control)
−4
−3
−2
−1
0
1
2
All Enhancers
Static Enhancers
Activated Enhancers
"Super" Enhancers
N = 12,391
N = 1,224
N = 1,709
N = 3,426
Brg1 unbound
N = 222
N = 507
N = 477
Brg1 bound

Fig S7

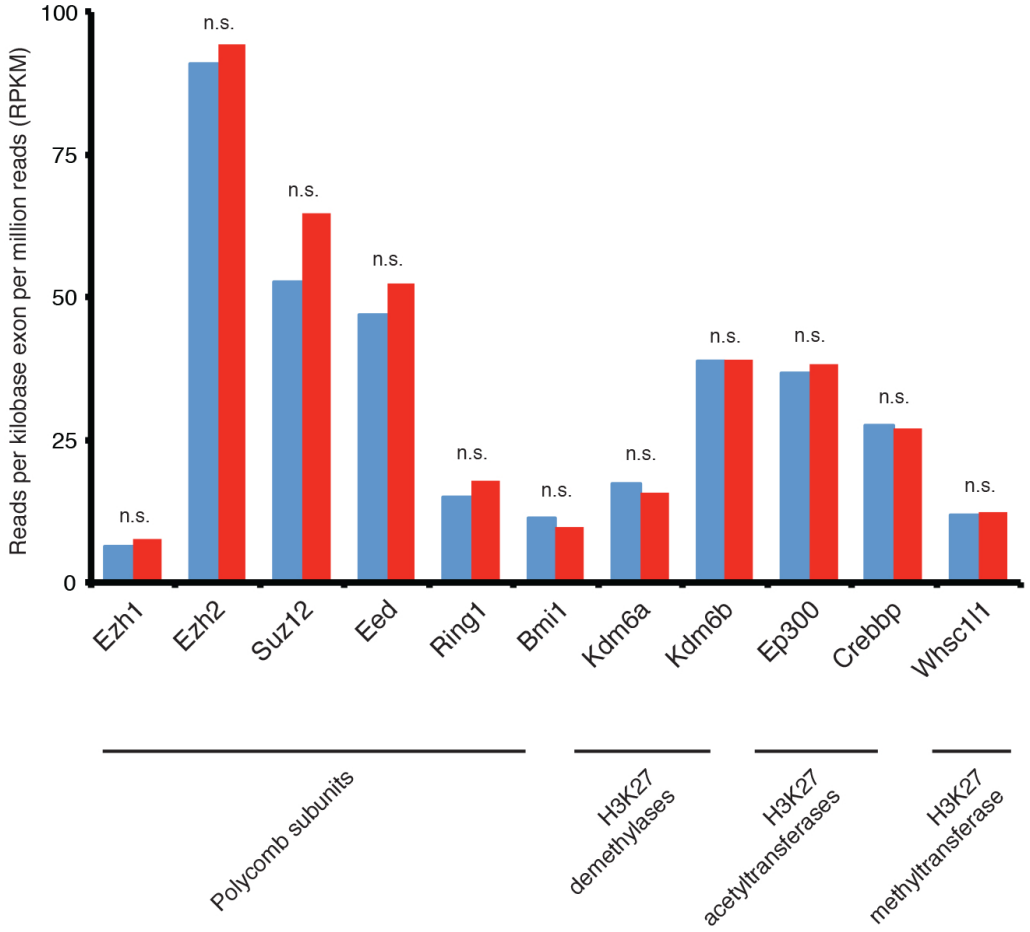
Reads per kilobase exon per million reads (RPKM)
100
75
50
25
0
n.s.
Ezh1
Ezh2
Suz12
Eed
Ring1
Bmi1
Kdm6a
Kdm6b
Ep300
Crebbp
Whsc1l1
Polycomb subunits
H3K27 demethylases
H3K27 acetyltransferases
H3K27 methyltransferase

Fig S8

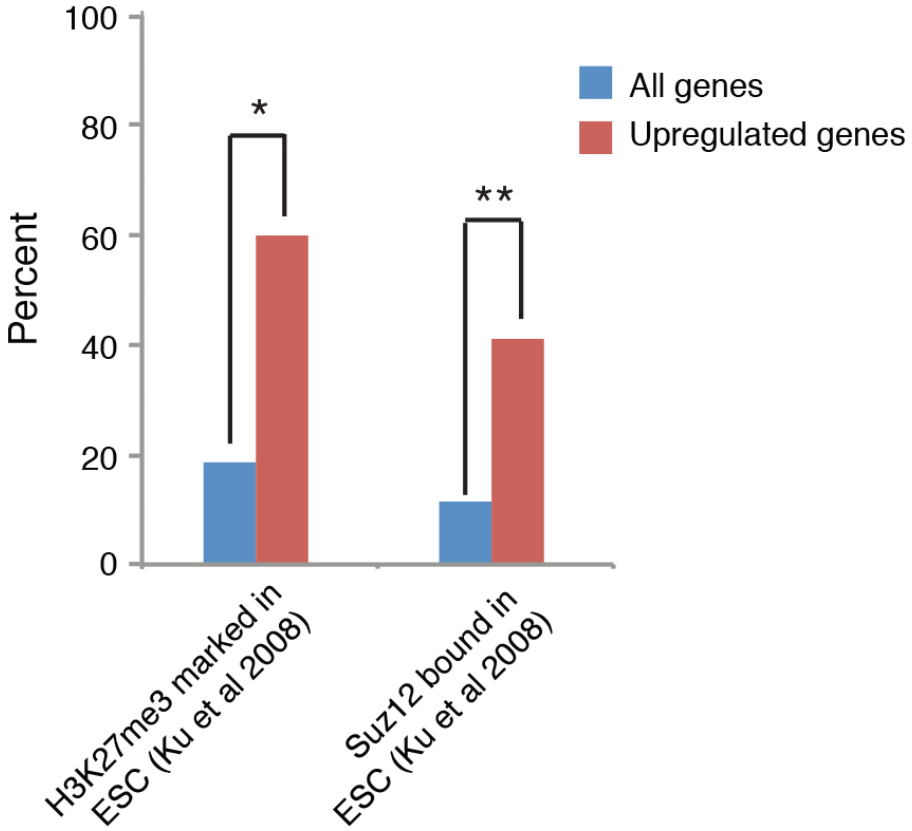
100
80
60
40
20
0
Percent
*
**
All genes
Upregulated genes
H3K27me3 marked in ESC (Ku et al 2008)
Suz12 bound in ESC (Ku et al 2008)

Supplementary Datasets

Table S1

Click here to Download Table S1

Table S2

Click here to Download Table S2

Table S3

Click here to Download Table S3

Table S4

Click here to Download Table S4